

1 Measurement report: Firework impacts on air quality in Metro Manila, Philippines during the
2 2019 New Year revelry

3 Genevieve Rose Lorenzo^{1,2}, Paola Angela Bañaga^{2,3}, Maria Obiminda Cambaliza^{2,3}, Melliza
4 Templonuevo Cruz^{3,4}, Mojtaba AzadiAghdam⁶, Avelino Arellano¹, Grace Betito³, Rachel
5 Braun⁶, Andrea F. Corral⁶, Hossein Dadashazar⁶, Eva-Lou Edwards⁶, Edwin Eloranta⁵, Robert
6 Holz⁵, Gabrielle Leung², Lin Ma⁶, Alexander B. MacDonald⁶, James Bernard Simpas^{2,3}, Connor
7 Stahl⁶, Shane Marie Visaga^{2,3}, Armin Sorooshian^{1,6}

8 ¹Department of Hydrology and Atmospheric Sciences, University of Arizona, Tucson, Arizona,
9 85721, USA

10 ²Manila Observatory, Quezon City, 1108, Philippines

11 ³Department of Physics, School of Science and Engineering, Ateneo de Manila University,
12 Quezon City, 1108, Philippines

13 ⁴Institute of Environmental Science and Meteorology, University of the Philippines, Diliman,
14 Quezon City, 1101, Philippines

15 ⁵Space Science and Engineering Center, University of Wisconsin - Madison, Madison,
16 Wisconsin, 53706, USA

17 ⁶Department of Chemical and Environmental Engineering, University of Arizona, Tucson,
18 Arizona, 85721, USA

19 *Correspondence to: armin@email.arizona.edu*

20 Abstract

21 Fireworks degrade air quality, reduce visibility, alter atmospheric chemistry, and cause short-
22 term adverse health effects. However, there have not been any comprehensive physicochemical
23 and optical measurements of fireworks and their associated impacts in a Southeast Asia
24 megacity, where fireworks are a regular part of the culture. Size-resolved particulate matter (PM)
25 measurements were made before, during, and after New Year 2019 at the Manila Observatory in
26 Quezon City, Philippines, as part of the Cloud, Aerosol, and Monsoon Processes Philippines
27 Experiment (CAMP²Ex). A High Spectral Resolution Lidar (HSRL) recorded a substantial
28 increase in backscattered signal associated with high aerosol loading ~440 m above the surface
29 during the peak of firework activities around 00:00 (local time). This was accompanied by PM_{2.5}
30 concentrations peaking at 383.9 $\mu\text{g m}^{-3}$. During the firework event, water-soluble ions and
31 elements, which affect particle formation, growth, and fate, were mostly in the submicrometer
32 diameter range. Total ($> 0.056 \mu\text{m}$) water-soluble bulk particle mass concentrations were
33 enriched by 5.7 times during the fireworks relative to the background (i.e., average of before and
34 after the firework). The water-soluble mass fraction of PM_{2.5} increased by 18.5% above that of
35 background values. This corresponded to increased volume fractions of inorganics which
36 increased bulk particle hygroscopicity, kappa (κ), from 0.11 (background) to 0.18 (fireworks).
37 Potassium and non-sea salt (nss) SO_4^{2-} contributed the most (70.9%) to the water-soluble mass,
38 with their mass size distributions shifting from a smaller to a larger submicrometer mode during
39 the firework event. On the other hand, mass size distributions for NO_3^- , Cl^- , and Mg^{2+} (21.1%
40 mass contribution) shifted from a supermicrometer mode to a submicrometer mode. Being both
41 uninfluenced by secondary aerosol formation and constituents of firework materials, a subset of
42 species were identified as the best firework tracer species (Cu, Ba, Sr, K^+ , Al, and Pb). Although
43 these species (excluding K^+) only contributed 2.1% of the total mass concentration of water-
44 soluble ions and elements, they exhibited the highest enrichments (6.1 to 65.2) during the
45 fireworks. Surface microscopy analysis confirmed the presence of potassium/chloride-rich cubic
46 particles along with capsule-shaped particles in firework samples. The results of this study
47 highlight how firework emissions change the physicochemical and optical properties of water-
48 soluble particles (e.g., mass size distribution, composition, hygroscopicity, and aerosol
49 backscatter), which subsequently alters the background aerosol's respirability, influence on
50 surroundings, ability to uptake gases, and viability as cloud condensation nuclei (CCN).

51 1. Introduction

52 Fireworks affect local populations through visibility reduction and increased health risks due to
53 briefly elevated particulate matter (PM) levels. Total PM mass concentrations during local
54 celebrations in the following cities exceeded the 24 h U.S. National Ambient Air Quality
55 Standard (NAAQS) for PM₁₀ of 150 µg m⁻³: Leipzig, Germany, (Wehner et al., 2000), Texas,
56 United States [U.S.], (Karnae, 2005), Montreal, Canada (Joly et al., 2010), and New Delhi, India,
57 (Mönkkönen et al., 2004). Firework emissions from at least nineteen studies have also been
58 linked to exceedance of the 24 h U.S. NAAQS limit for PM_{2.5} of 35 µg m⁻³ (Lin, 2016 and
59 references therein). Higher PM concentrations from fireworks have been reported more
60 frequently in Asia (i.e., India, China, and Taiwan) compared to Western countries (Lin, 2016;
61 Sarkar et al., 2010).

62 Health effects are of major concern during firework periods based on both short and long-term
63 exposure. For example, Diwali is a major firework festival in India, and it was shown that
64 chronic exposure to three of the most prominent tracer species (Sr, K, and Ba) translated to a 2%
65 increase in health effects based on the non-carcinogenic hazard index (Sarkar et al., 2010). On
66 the other hand, short term exposure to firework pollutants increases asthma risk, eye allergies,
67 cardiovascular and pulmonary issues, cough, and fever (Moreno et al., 2010; Singh et al., 2019;
68 Barman et al., 2008; Becker et al., 2000; Beig et al., 2013; Hirai et al., 2000). Firework pollutants
69 also impact clouds and the hydrological cycle, owing to associated aerosols serving as cloud
70 condensation nuclei (CCN) (Drewnick et al., 2006) and subsequently impacting surface
71 ecosystems after wet deposition (Wilkin et al., 2007). Although fireworks emit particles with
72 various sizes into the atmosphere, fine particles associated with PM_{2.5} are most relevant to public
73 health effects, scattering efficiency, and CCN activation (Vecchi et al., 2008; Perry, 1999).
74 Knowing the various effects of firework emissions depends on knowing their physical, chemical,
75 and optical properties.

76 Measurements of the chemical composition of firework emissions are important in order to
77 understand how they affect local air quality. The main components of fireworks are fuels (metals
78 and alloys, metalloids, and non-metals), oxidizers (nitrates, perchlorates, and chlorates), and
79 coloring agents (metal salts) (Steinhauser and Klapotke, 2010). Previous studies have relied on
80 tracer species to establish confidence in distinguishing the firework source from background air
81 and other sources (Sarkar et al., 2010). Potassium historically has been the most observable
82 tracer for fireworks emissions (Wang et al., 2007; Drewnick et al., 2006; Perry, 1999), with
83 concentrations reaching 58 µg m⁻³ during the Diwali Festival in India (Kulshrestha et al., 2004).
84 Firework color is created by metal salts such as Sr for red, Ba for green, and Cu for blue, all
85 three of which have and have been found to be effective tracers of fireworks (Walsh et al., 2009;
86 Vecchi et al., 2008). Strontium in particular is an indicator of the spatial and temporal extent of
87 firework smoke plumes (Perry, 1999) because of the high prevalence of red in fireworks and it is
88 not affected by traffic emissions (Moreno et al., 2010). Other components measured in the air that
89 have been attributed to fireworks include metals (Al, Cd, Cu, Ti, Mg, Mn, Ni, Zn, As, Bi, Co,
90 Ga, Hg, Cr, Pb, Rb, Sb, P) and their salt anion counterparts (S, P, Cl). Also from fuel and
91 oxidizer combustion are species such as NO₃⁻, SO₄²⁻, and organics including oxaloacetic acid
92 (Alpert and Hopke, 1981; Barman et al., 2008; Carranza et al., 2001; Dorado et al., 2001;

93 Drewnick et al., 2006; Joly et al., 2010; Joshi et al., 2016; Kulshrestha et al., 2004; Kumar et al.,
94 2016; Lin et al., 2016; Moreno et al., 2010; Sarkar et al., 2010; Tanda et al., 2019; Thakur et al.,
95 2010; Joshi et al., 2019). Firework-derived chloride in Taiwan has been attributed to raw
96 materials such as KClO_3 , ClO_3 , and ClO_4 with $\text{Cl}^-:\text{Na}^+$ ratios reaching approximately 3 (Tsai et
97 al., 2012). Black carbon mass concentrations during firework events can either increase due to
98 firework emissions or decrease owing to fewer vehicles on the road (Kumar et al., 2016; Yadav
99 et al., 2019). In both cases, the black carbon mass fraction decreases due to a greater contribution
100 of other constituents in firework emissions. Organic mass concentrations and mass fractions have
101 been noted to increase and decrease, respectively, with fireworks (Zhang et al., 2019). Governed
102 largely by composition, particulate hygroscopicity and solubility have also been found to be
103 altered by fireworks depending on the emitted species. Inorganic salts (K_2SO_4 , KCl) dominated
104 the aerosol hygroscopicity in Xi'an, China during fireworks (Wu et al., 2018). In the
105 Netherlands, enhancements in salt mixtures containing SO_4^{2-} , Cl^- , Mg^{2+} , and K^+ were noted to
106 enhance hygroscopicity (ten Brink et al., 2018). Copper and Mg were observed to become more
107 soluble in firework emissions in Delhi, India, while Mn, As, Ba, and Pb became less soluble
108 (Perrino et al., 2011). The water-soluble aerosol component from fireworks in Sichuan Basin
109 (China) were internally mixed and enhanced the hygroscopicity of submicrometer aerosols,
110 especially the larger particles (Yuan et al., 2020).

111 In addition to composition, a necessary aspect of characterizing impacts of firework emissions is
112 to measure aerosol size distributions within the short timeframe of an event (Joshi et al., 2019).
113 Owing to combustion during firework events, PM concentrations are dominated by particles in
114 the submicrometer range (Vecchi et al., 2008; Nicolás et al., 2009; Joshi et al., 2019; Pirker et
115 al., 2020; Do et al., 2012). Particle number concentration maxima have been noted for the
116 nucleation (0.01 to 0.02 μm) and Aitken (0.02 to 0.05 μm) modes (Yadav et al., 2019; Yuan et
117 al., 2020), in addition to both the small (0.1 to 0.5 μm) (Wehner et al., 2000; Zhang et al., 2010)
118 and large (0.5 to 1.0 μm) ends of the accumulation mode (Vecchi et al., 2008) during firework
119 events. In Nanning, China, SO_4^{2-} peaked at 0.62 μm during fireworks (Li et al., 2017). The mass
120 diameter of K^+ was 0.7 μm due to firework emissions after transport in Washington State (Perry,
121 1999). There are a few studies with observed particle mass concentration increases in the coarser
122 but still respirable (< 10 μm) mode (Tsai et al., 2011). In terms of dynamic behavior in the size
123 distributions, past work has shown a shift in number concentration from nucleation and Aitken
124 modes to the smaller end of the accumulation mode (0.1 to 0.5 μm), due to increased coagulation
125 sinks (Zhang et al., 2010). Finer temporal scale monitoring has revealed steep increases in
126 nucleation mode and Aitken mode particle concentrations associated with firework emissions
127 followed by a growth in accumulation mode particle number concentrations due to coagulation
128 (Yadav et al., 2019). An opposite shift to a smaller size distribution has been observed for certain
129 species (Mg, Al, Cu, Sr, and Ba) from the coarse mode to accumulation mode (Tanda et al.,
130 2019). Other work has shown that while there is usually a quick drop in particle concentration to
131 background values after firework events (Joly et al., 2010), elevated number concentrations of
132 accumulation mode particles are maintained for up to three hours after peak firework activity
133 (Hussein et al., 2005). New particle formation events with fireworks have also been reported in

134 Mumbai, India (Joshi et al., 2016), with enrichments of primary and secondary particles for up to
135 30 minutes after peak firework activity. Particle aging due to distance from the source and
136 meteorology alter firework emission particle concentrations (Joly et al., 2010) and size
137 distributions (Khaparde et al., 2012).

138 Meteorological and dynamic parameters such as wind speed, level of mixing (turbulent kinetic
139 energy), and mixing layer height (Lai and Brimblecombe, 2020) influence peak concentration
140 and composition of aerosols after fireworks, as well as particle residence time in the atmosphere
141 and transport to nearby regions (Vecchi et al., 2008). Although firework activities are episodic,
142 their particulate emissions, especially in the submicrometer mode (Do et al., 2012), reside in the
143 atmosphere for as long as several days to weeks (Liu et al., 1997; Lin et al., 2016; Kong et al.,
144 2015; Do et al., 2012). Dispersion of the particles under low wind speed (1 m s^{-1}) for particles
145 between 0.4 and $1 \mu\text{m}$ is estimated at 12 h (Vecchi et al., 2008) and can reach distances as far as
146 a hundred kilometers (Perry, 1999). Aitken mode and larger particles are dispersed by wind more
147 than nucleation-mode particles (Agus et al., 2008). Meteorological conditions, such as rainfall,
148 can also decrease firework particle loading in the air and relative humidity can change the
149 hygroscopicity of firework emissions (Hussein et al., 2005), thereby affecting their size and
150 radiative properties.

151 Studies on aerosol properties are limited for the rapidly developing region of Southeast Asia
152 (Tsay et al., 2013). This compounds the challenge to understand the interactions between
153 aerosols and the complex hydro-meteorological and geological environment in Southeast Asia
154 (Reid et al., 2013). Increased local and transported emissions (Hopke et al., 2008; Oanh et al.,
155 2006) in Southeast Asia add to the complexity and affect air quality in the region. Firework
156 emissions are an example of extreme and regular local emissions in Southeast Asia. Even while
157 several studies exist in the neighboring regions of East Asia (e.g., China) and South Asia (e.g.,
158 India), there currently is no in-depth analysis of the chemical, physical, and optical properties of
159 firework emissions in a Southeast Asian megacity where fireworks are culturally significant. This
160 study is additionally novel because it includes the following combination of data types to
161 investigate fireworks: size-resolved measurements (ionic/elemental composition, morphology),
162 vertically-resolved data from a High Spectral Resolution Lidar (HSRL), $\text{PM}_{2.5}$, and meteorology.
163 This work reports these data during the 2019 New Year celebrations in Metro Manila,
164 Philippines, one of the most populated cities, with 12.88 M population (PSA, 2015). We address
165 the following questions in order: (i) what are the conditions of the atmosphere during the study
166 period in relation to aerosols, and how are these affected by firework emissions?; (ii) what are
167 the concentrations, mass size distributions, and morphological characteristics of different
168 elemental and ionic species specific to fireworks, and how do these affect bulk aerosol
169 hygroscopicity? The results of this work provide new data that can help address how past and on-
170 going firework emissions impact health, visibility, regional air quality, and biogeochemical
171 cycling of nutrients and contaminants in the Philippines, Southeast Asia, and, more broadly, for
172 all other cities with major firework events. It also contributes to the growing body of firework
173 research findings (Devara et al., 2015).

174

175 **2. Methods**

176 2.1 Hourly PM_{2.5} Mass Concentration

177 Hourly PM_{2.5} mass concentrations were obtained to assess the evolution of and the temporal
178 characteristics of fine particulates due to fireworks and their relation to meteorology and aerosol
179 optical properties. The hourly PM_{2.5} mass concentrations were collected at the Manila
180 Observatory, Quezon City, Philippines (14.64° N, 121.08° E, ~70 m. a. s. l.) (Fig. S1) with a beta
181 attenuation monitor (DKK-TOA Corporation) as part of the East Asia Acid Deposition
182 Monitoring Network (EANET) (Totsuka et al., 2005). The beta attenuation monitor collects
183 PM_{2.5} samples on a ribbon filter, which are irradiated with beta particles. The attenuation of the
184 beta particles through the sample and the filter is exponentially proportional to the mass loading
185 on the filter. These hourly data were then averaged over 48-hour periods coinciding with water-
186 soluble aerosol composition measurements (Section 2.5) before, during, and after the firework
187 event.

188

189 2.2 Meteorological Data

190 Rainfall, temperature, relative humidity, and wind data were collected at the Manila Observatory
191 with a Davis Vantage Pro2 Plus weather station (~90 m. a. s. l) before, during, and after the
192 firework period. Hourly precipitation accumulation and 10-min averaged temperature, relative
193 humidity, and wind were used for the analysis.

194

195 2.3 Back Trajectories

196 Three-day back trajectories with six-hour resolution were generated using the National Oceanic
197 and Atmospheric Administration's (NOAA) Hybrid Single-Particle Lagrangian Integrated
198 Trajectory (HYSPLIT) model (Rolph et al., 2017; Stein et al., 2015) using the Global Data
199 Assimilation System (GDAS) with a resolution of 1°, and vertical wind setting of "model vertical
200 velocity". To ascertain the impact of fireworks on surface particulate concentrations, back
201 trajectories were chosen to end at the beginning times of the sampling periods before, during,
202 and after the firework event. Trajectories were computed for an end point being at the Manila
203 Observatory at an altitude of 500 m because it represents the mixed layer as done in other works
204 examining surface air quality (Mora et al., 2017; Aldhaif et al., 2020; Crosbie et al., 2014;
205 Schlosser et al., 2017).

206

207 2.4 Remote Sensing

208 Vertical profiles of aerosol backscatter cross-section measured with the University of Wisconsin
209 High Spectral Resolution Lidar (HSRL) which was deployed at the Manila Observatory in

210 support of CAMP²EX. The HSRL instrument transmitting laser (Table S1) operates at 532 nm
211 with 250 mW average power and pulse repetition rate of 4 KHz. The HSRL technique measures
212 and separates the returned signal into the molecular and aerosol backscatter by using a beam
213 splitter and an iodine absorption cell filter. The separated molecular signal allows for optical
214 depth and backscatter cross section measurements in contrast to a standard backscatter lidar that
215 requires assumption related to the particulate lidar ratio (Razenkov, 2010). The HSRL also
216 measures particulate depolarization ratio, an indicator of aerosol or cloud particle shape with low
217 depolarization indicative of spherical particles while intermediate values (10%) indicate a mix of
218 spherical and nonspherical particles (Burton et al., 2014; Reid et al., 2017). HSRL data were
219 uploaded and processed at the University of Wisconsin-Madison Space Science and Engineering
220 Center server for periods before, during, and after the fireworks.

221 To verify the height values based on the vertical profiles of aerosol backscatter, the “surface-
222 attached aerosol layer” height is estimated using the maximum variance method more commonly
223 used for daytime convective boundary layer detection (Hooper and Eloranta, 1986). The height
224 detection method is limited by the complexity of the firework event case due, however, to
225 pertinent rain signals. The “surface attached aerosol layer” is derived from a 15-min moving
226 window average based on the 30-s values.

227

228 2.5 Aerosol Composition and Morphology Measurements

229 Size-speciated PM (cut-point diameters: 18, 10, 5.6, 3.2, 1.8, 1.0, 0.56, 0.32, 0.18, 0.10, and
230 0.056 μm) was collected on Teflon substrates (PTFE membrane, 2 μm pores, 46.2 mm diameter,
231 Whatman) with two Micro-Orifice Uniform Deposition Impactor (MOUDI II 120R, MSP
232 Corporation) (Marple et al., 2014) samplers from the third floor of the main building (~85 m. a.
233 s. l) at the Manila Observatory. Sample collection for each of the three MOUDI sets lasted 48
234 hours before (13:30 December 24, 2018 to 13:30 December 26, 2018), during (14:45 December
235 31, 2018 to 14:45 January 2, 2019), and after (13:30 January 1, 2019 to 13:30 January 3, 2019)
236 firework activities. Note all times refer to local time (UT + 8 hours). Although there were no
237 fireworks released from the sampling site, there was firework activity in the immediate vicinity
238 (~ 500 m from the sampling in all directions and all throughout the city in general). Firework
239 activity around the sampling site began around ~19:00 on 31 December 2018, peaked at 00:00 of
240 1 January 2019, and dropped drastically after. Based on PM_{2.5} data there was no evidence of
241 sustained firework activity past midnight. MOUDI samples collected before (December 24 to 26)
242 and after (January 1 to 3) the firework event (December 31 to January 2) were considered as
243 background samples. Although there is some firework activity that is expected in the evening of
244 December 24 (before the firework event), this is minimal compared to that which is the focus of
245 this study. The samples were covered with aluminum foil, sealed, and stored in the freezer before
246 being shipped to the University of Arizona for elemental and ionic analysis.

247 Each sample substrate was cut in half. One half of each sample was extracted in 8 mL Milli-Q
248 water (18.2 M Ωcm), sonicated, and analyzed for ions (ion chromatography (IC): Thermo
249 Scientific Dionex ICS-2100 system) and elements (triple quadrupole inductively coupled plasma

250 mass spectrometer: ICP-QQQ; Agilent 8800 Series). The remaining substrate halves were stored.
251 Sample ionic and elemental concentrations were corrected by subtracting concentrations from
252 background control samples. More information about the sampling and analysis are detailed in
253 recent work (Stahl et al., 2020b). Limits of detection of the forty-one reported species are
254 summarized in Table S3. Potassium (K^+) was reported based on ICP-QQQ measurements rather
255 than IC due to possible contamination from the KOH eluent used in the latter instrument. Non-
256 sea salt SO_4^{2-} was calculated by subtracting $0.2517 * Na^+$ from the total SO_4^{2-} concentration
257 (Prospero et al., 2003).

258 High-resolution scanning electron microscopy (SEM) combined with energy dispersive X-ray
259 analysis (EDX) was used for examining particle morphology and chemical composition on a
260 portion of the substrates collected during the firework event. Analyses were performed with a
261 Hitachi S-4800 high-resolution SEM and a Thermo Fisher Scientific Noran Six X-ray
262 Microanalysis System in the Kuiper Imaging cores at the University of Arizona. Approximately
263 1 cm^2 was cut from the center of substrate halves and placed on double-sided carbon tape
264 mounted on an aluminum stub. A thin layer (1.38 nm) of carbon was coated on the sample
265 surface using a Leica EM ACE600 sputter coater to improve the sample's conductivity. SEM
266 images were obtained at 15 keV and 30 keV acceleration voltages and with a $20\text{ }\mu\text{A}$ probe
267 current in high-magnification mode. The percentage contributions and the spatial distribution of
268 the elements were obtained from the EDX analysis. Carbon, F, and Al should be ignored in the
269 discussion of SEM-EDX results since C and F are present in the Teflon substrates, and the
270 sample stub is an Al-rich substrate.

271 A total of 41 water-soluble species were detected in the 48-hr size-differentiated particulate
272 samples collected before, during, and after the firework event. The total bulk mass concentration
273 is defined as the sum of the concentrations of all the measured species across the MOUDI's
274 eleven stages ($\geq 0.056\text{ }\mu\text{m}$).

275 276 2.6 Enrichment Factor Calculations

277 To identify which species are most enhanced during fireworks, enrichment values are typically
278 calculated using speciated concentrations during the fireworks relative to baseline periods
279 (Tanda et al., 2019). We calculate water-soluble mass enrichment factors for each of the forty-
280 one measured species by dividing their total bulk ($\geq 0.056\text{ }\mu\text{m}$) mass concentrations during the
281 firework event by the average of the total mass concentration of the species measured before and
282 after the firework event. Size-resolved enrichments were similarly calculated using measured
283 mass concentrations for individual MOUDI stages. In a case when the mass concentration of a
284 species during the firework event was non-zero but the mass concentrations during and after
285 were zero (e.g., succinate), half of the detection limit was used in place of zero values.

286 287 2.7 Hygroscopicity Calculations

288 Hygroscopicity was calculated for particles ranging in size between 0.056 – 3.2 μm before,
289 during, and after the firework event. This size range was chosen to most closely be aligned with
290 separate measurements of $\text{PM}_{2.5}$ in the study (Section 2.1) that were used to account for the
291 remaining mass not speciated in this study. We specifically calculate values for the single
292 hygroscopicity parameter kappa, κ (Petters and Kreidenweis, 2007).

293 The water-soluble compound mass concentrations before, during, and after the firework event
294 were calculated using an ion-pairing scheme (Gysel et al., 2007) for each MOUDI stage between
295 diameters of 0.056 and 3.2 μm , and then summed to achieve a total mass concentration for each
296 compound in this size range. Black carbon mass concentrations in $\text{PM}_{2.5}$ before and after the
297 firework event were calculated based on their long-term (2001-2007) average contribution (32%)
298 to $\text{PM}_{2.5}$ mass in December and January (Cohen et al., 2009). Black carbon or elemental carbon
299 (EC) concentrations during the firework event were assumed to be the average of the black
300 carbon concentrations before and after the firework event. This was done because black carbon
301 concentrations have been observed to not increase (Santos et al., 2007) as much as organic
302 carbon (OC) (Lin, 2016), such that OC:EC mass ratios during fireworks have been observed to
303 increase. Total non-water-soluble content between 0.056 and 3.2 μm was calculated as the
304 difference between the total $\text{PM}_{2.5}$ mass concentration and the sum of the water-soluble species
305 and black carbon mass concentrations. The mass of each species was divided by its density, and
306 each of these volumes were added to quantify the volume of the measured aerosol (water-soluble
307 compounds, black carbon, and organic matter) between 0.056 and 3.2 μm . Volume fractions
308 were then computed for each species. The Zdanovskii, Stokes, and Robinson (ZSR) mixing rule
309 (Stokes and Robinson, 1966) was used to obtain the total hygroscopicity (total κ) of the mixed
310 aerosols by weighting κ values for the individual non-interacting compounds by their respective
311 volume fractions and summing linearly. Densities and κ values for the individual compounds are
312 based on those used elsewhere (AzadiAghdam et al., 2019), repeated in Table S4.

313

314 **3. Results and Discussion**

315 **3.1 Hourly $\text{PM}_{2.5}$, Meteorological, and Transport Patterns**

316 We begin with hourly $\text{PM}_{2.5}$ mass concentration results for the study period to provide context
317 for the spatio-temporal characteristics of fine particulates due to fireworks, their interaction with
318 meteorology, and effects on aerosol optical properties. Hourly $\text{PM}_{2.5}$ (Fig. 1) began to increase
319 from 44.0 $\mu\text{g m}^{-3}$ (shortly after rising above the 24-h Philippine National Ambient Air Quality
320 Guideline Value (NAAQGV) of 50.0 $\mu\text{g m}^{-3}$) after 18:00 time on 31 December 2018 with the
321 beginning of firework activity and calm meteorological conditions. There was moderate (3 mm)
322 rainfall from 22:00 to 23:00 that night as the firework activity began to increase. Rain is a sink
323 for particles (Perry, 1999) and could have washed out some of the particulates in the air, thus
324 potentially causing a slight dip in the hourly $\text{PM}_{2.5}$ around midnight. $\text{PM}_{2.5}$ peaked at 383.9 $\mu\text{g m}^{-3}$
325 between 01:00 to 02:00 on 1 January 2019. The $\text{PM}_{2.5}$ peak was delayed by approximately an
326 hour from the peak firework activity at midnight possibly due to rainfall, relative humidity, and

327 wind (Vecchi et al., 2008), in addition to aerosol dynamical processes requiring time for
328 secondary aerosol formation and growth (Li et al., 2017). Minimal rain (0.2 mm in an hour) with
329 high relative humidity (between $93\% \pm 4\%$ to $94\% \pm 4\%$) were conducive to aerosol growth
330 and/or secondary particle formation. High relative humidity is related to aqueous-phase oxidation
331 of SO_2 (Sun et al., 2013) and NO_2 (Cheng et al., 2014) as well as metal-catalyzed heterogeneous
332 reactions (Wang et al., 2007) to form SO_4^{2-} . Aqueous oxidation has been found to be a
333 predominant mechanism for the secondary formation of SO_4^{2-} during fireworks (Li et al., 2017),
334 in addition to promoting secondary organic aerosol formation (Wonaschuetz et al., 2012; Youn
335 et al., 2013). Light wind ($\sim 1 \text{ m s}^{-1}$) after midnight from the northeast could also have transported
336 more emissions from the populated Marikina Valley, located in the northeast, to the Manila
337 Observatory contributing to the delay of the $\text{PM}_{2.5}$ peak.

338 Particulate levels were enhanced for approximately 14 h from the beginning of the firework
339 activity (Fig. 1) during which the average $\text{PM}_{2.5}$ ($143.4 \mu\text{g m}^{-3}$) exceeded the 24 h Philippine
340 NAAQGV between 18:00 on 31 December 2018 to 08:00 on 1 January 2019. After 02:00 on 1
341 January 2019, $\text{PM}_{2.5}$ dropped quickly to $122.0 \mu\text{g m}^{-3}$ between 03:00 to 04:00 (Fig. 1). The $\text{PM}_{2.5}$
342 decrease was less pronounced after 04:00 but continued decreasing steadily along with slight rain
343 (0.4 mm in an hour) and light breeze ($1 - 2 \text{ m s}^{-1}$) from the northwest to southwest directions.
344 Firework activity in other countries have been documented to last from 2 – 6 h in a day and
345 elevated particulate levels can be maintained for up to 6 – 18 h (Thakur et al., 2010; Crespo et
346 al., 2012; Chatterjee et al., 2013; Kong et al., 2015; Tsai et al., 2012). The 48-h average $\text{PM}_{2.5}$
347 during ($49.9 \mu\text{g m}^{-3}$) the firework event was 1.9 and 3.3 times more, respectively, than before
348 ($25.8 \mu\text{g m}^{-3}$) (Fig. S2) and after ($15.2 \mu\text{g m}^{-3}$) (Fig. S3) the firework event. Two to three-fold
349 increases in PM mass concentration due to fireworks have also been observed in other countries
350 (Rao et al., 2012; Ravindra et al., 2003; Tsai et al., 2011; Shen et al., 2009). Greater increases ($>$
351 5 times) in particulate mass concentrations elsewhere were related to more intense and prolonged
352 (lasting several days) firework activity (Tian et al., 2014).

353 Three-day back trajectories for the period before the firework event were from the northeast to
354 east directions coming from the Philippine Sea (Fig. 2a). For the periods (Fig. 2b) during and
355 (Fig. 2c) after the firework event, back trajectories were from the northeast to east/northeast
356 directions. The general wind directions from the back trajectories are consistent with the
357 climatologically prevailing northeasterly monsoonal winds in December and January for the
358 Philippines (Villafuerte II et al., 2014). The origin of the air parcels did not have any major
359 emissions events that could have impacted the measurements after long-range transport. This is
360 important to note because the tracers for fireworks are also tracers for transported emissions due
361 to biomass burning (K^+) (Braun et al., 2020) and industrial activities (Cohen et al., 2009). Thus,
362 enriched particulate concentrations during the firework activity were most likely locally
363 produced. One factor impacting surface PM concentrations is the vertical structure of the lower
364 troposphere, which is addressed in the next section based on HSRL data.

365

366 3.2 Optical Aerosol Properties

367 Heavy aerosol loading at the surface was observed up to eight hours after the fireworks peak
368 (00:00) with high HSRL 532 nm backscatter cross-section and depolarization (Fig. 3a) reaching
369 ~440 m above the ground. Prior to the firework peak, the surface aerosol layer had lower
370 backscatter (before 22:00, Fig. 3a), and this cleaner condition is shown by the 16:16 local time
371 vertical profile of the aerosol backscatter (Fig. 3b). Rainfall (Fig. 1a) contributed to columns of
372 high backscatter (Fig. 3a) after 22:00 and before the firework peak with a measurable decrease in
373 the aerosol backscatter for a short time after the precipitation (23:00 and 00:00).

374 As confirmed by height detection, aerosols reached up to ~440 m (Fig 3a and b) at 00:00 (1
375 January 2019). It persisted for at least an hour then dropped to 118 ± 20 m with higher aerosol
376 backscatter retained until January 1, 2019 08:00. Some of the smoke is above the detected height
377 (i.e. 01:00).

378

379 3.3 Mass Size Distributions

380 Building on the previous results describing the general environmental conditions during the
381 study period, now we focus on the detailed size-resolved measurements. The total water-soluble
382 bulk mass concentration (Table 1) during the firework event ($16.74 \mu\text{g m}^{-3}$) was 5.71 times and
383 4.73 times higher than the total bulk mass concentrations before ($2.93 \mu\text{g m}^{-3}$) and after ($3.54 \mu\text{g}$
384 m^{-3}) the firework event, respectively. Assuming the average of the water-soluble mass
385 concentrations before and after the firework event represent background values, this translates to
386 an 80.66% increase in water-soluble mass during the firework event.

387 The firework event was associated with increased total water-soluble mass fraction (32.33%)
388 ($0.056 - 3.2 \mu\text{m}$ size range, Section 3.1) in $\text{PM}_{2.5}$ (Fig. S4) compared to before (9.90%) and after
389 (17.79%) the firework event. The water-soluble particulate mass fraction in $\text{PM}_{2.5}$ similarly
390 increased in other firework events (Yang et al., 2014). The highest total water-soluble mass
391 concentrations during the firework event were from the following ions: non-sea salt (nss) SO_4^{2-}
392 ($6.81 \mu\text{g m}^{-3}$), K^+ ($5.05 \mu\text{g m}^{-3}$), NO_3^- ($1.70 \mu\text{g m}^{-3}$), Cl^- ($1.46 \mu\text{g m}^{-3}$), Mg^{2+} ($0.37 \mu\text{g m}^{-3}$), Na^+
393 ($0.33 \mu\text{g m}^{-3}$), and Ca^{2+} ($0.30 \mu\text{g m}^{-3}$). These contributed to 95.75% of the total detected bulk
394 water-soluble mass concentration then.

395 Total water-soluble bulk mass concentration during the firework event was dominated by
396 submicrometer particles, which accounted for 77.4% of the total water-soluble bulk mass (Fig.
397 4b). Supermicrometer mass fractions were greater before (Fig. 4a) and after (Fig. 4c) the
398 firework event (43.7% and 57.5% of the water-soluble bulk mass concentration) compared to
399 during the firework event (22.6%). The increase in submicrometer mass fractions is typical with
400 firework emissions (Crespo et al., 2012; Do et al., 2012). In New York, fireworks contributed to
401 77% of PM_1 due to potassium salts and oxidized organic aerosol (Zhang et al., 2019).

402 Non-sea salt SO_4^{2-} had the highest contribution (40.7%) to total water-soluble bulk mass
403 concentration during the firework event (Table 1). Sulfate exhibited a shift in its mass size
404 distribution to a slightly larger size during firework activity (Fig. 4b). During the firework event,
405 87.13 % of the nss- SO_4^{2-} was in the 0.32 μm to 1.8 μm size fraction. Before and after the
406 firework event, 87.28% and 85.14% of the nss- SO_4^{2-} mass concentration, respectively, was
407 distributed in a finer size fraction (0.18 μm to 1 μm) (Fig. 4a and 4c).

408 Potassium contributed 30.19% to the total water-soluble mass concentration during the firework
409 event (Table 1), presumably in the form of KNO_3 . This compound is associated with black
410 powder used as a propellant (Li et al., 2017). Potassium's mass concentration distribution
411 similarly shifted to a slightly larger size during the firework event (Figure 4b). Most (87.6%) of
412 the bulk K^+ mass concentration during the firework event was between 0.32 and 1.8 μm ,
413 compared to 85.4% and 79.4% between 0.18 and 1 μm before and after the firework event,
414 respectively (Fig. 4a and 4c).

415 The shift in the mass size distribution of K^+ and nss- SO_4^{2-} can be due to the removal of
416 nucleation-mode particles as a result of increased coagulation in the accumulation mode (Zhang
417 et al., 2010). Relatively larger SO_4^{2-} particles can also be due to secondary sources rather than
418 primary sources, and aging could have also contributed to particle growth as has been suggested
419 for firework particles in Nanning, China (Li et al., 2017). Firework emissions include gases like
420 SO_2 which undergo aqueous uptake and oxidation onto particles to form SO_4^{2-} . Furthermore,
421 enhanced secondary formation is aided by metals emitted during fireworks that help convert SO_2
422 to SO_4^{2-} (Feng et al., 2012; Wang et al., 2007).

423 Nitrate, Cl^- , and Mg^{2+} mass size distributions all exhibited pronounced peaks in the
424 submicrometer range during the firework event (Fig. 5). The mass sum concentration of the
425 aforementioned ions peaked (46.39% of the total mass concentration of the three species)
426 between 0.56 and 1.0 μm . On the other hand, their mode appeared between 1.8 and 3.2 μm
427 before and after the firework event (33.02% and 32.91% of the total mass concentration of the
428 three species, respectively) (Fig. 5). Nitrate, Cl^- , and Mg^{2+} are emitted during fireworks (Zhang et
429 al., 2017) as finer-sized submicrometer particles (Tsai et al., 2011) compared to background
430 conditions when these species are mostly associated with coarser supermicrometer particles
431 (AzadiAghdam et al., 2019; Cruz et al., 2019; Hilario et al., 2020). Nitrate can also be formed
432 secondarily (Yang et al., 2014) from firework emissions. Firework emissions are associated with
433 lower $\text{NO}_3^-:\text{SO}_4^{2-}$ ratios (Feng et al., 2012) compared to days dominated by mobile sources
434 (Arimoto et al., 1996) due to different formation mechanisms (Tian et al., 2014). Consistent with
435 the literature, low $\text{NO}_3^-:\text{SO}_4^{2-}$ ratios were also observed during the firework event (before: 0.79,
436 during: 0.25, after: 0.82). A low $\text{NO}_3^-:\text{SO}_4^{2-}$ ratio is related to decreased pH of the particles (Cao
437 et al., 2020), which may impact not just air quality and health but also nearby waterbodies where
438 the particles may deposit. It is important to note that background supermicrometer Cl^- and Mg^{2+}
439 in Manila are most likely associated with sea salt while background supermicrometer NO_3^-
440 possibly in the form of NaNO_3 (de Leeuw et al., 2001) or NH_4NO_3 likely stems from partitioning
441 of nitric acid gas onto surfaces (de Leeuw et al., 2001) of coarse particles such as sea salt and

442 dust (AzadiAghdam et al., 2019; Cruz et al., 2019). The $\text{Cl}^-:\text{Na}^+$ mass ratio during the firework
443 event increased to 4.44 (from 0.69 and 1.08 before and after, respectively) and was higher than
444 the typical $\text{Cl}^-:\text{Na}^+$ ratio in seawater of 1.81 (Braun et al., 2017). These ratio results confirm that
445 the increase in Cl^- concentrations during the firework event is not driven by sea salt but instead
446 linked to firework emissions. The lack of increased sea salt influence during the firework event,
447 which is not to be expected, is further confirmed by relatively small changes in the amount of
448 observed Na^+ , as will be discussed subsequently.

449 The Na^+ , Ca^{2+} , and NH_4^+ mass size distributions peak in the supermicrometer range (1.8 to 3.2
450 μm) (Figure S5) and total mass concentrations (Table 1) varied minimally, relative to the earlier
451 mentioned species, before ($0.33 \mu\text{g m}^{-3}$, $0.21 \mu\text{g m}^{-3}$, $0.21 \mu\text{g m}^{-3}$, respectively), during ($0.33 \mu\text{g}$
452 m^{-3} , $0.30 \mu\text{g m}^{-3}$, $0.19 \mu\text{g m}^{-3}$) and after ($0.53 \mu\text{g m}^{-3}$, $0.38 \mu\text{g m}^{-3}$, $0.28 \mu\text{g m}^{-3}$) the firework
453 event. The minimal change in NH_4^+ mass concentration is most likely due to little or no variation
454 of its precursor gas (e.g., NH_3) due to firework activities and the fact that firework materials are
455 commonly composed of K-rich salts rather than NH_4^+ salts (Zhang et al., 2019). The latter seems
456 probable because the K:S mass ratios of 2.75 and 2.71, observed from 0.18 – 0.32 μm and 0.32 –
457 0.56 μm , respectively, during the firework event suggests a firework-related source of K and S.
458 This ratio is similar to the K:S ratio of 2.75 (Dutcher et al., 1999) of “black powder” (Perry,
459 1999), a type of pyrotechnic comprised of K and S.

460 The mass size distribution for the sum of the rest of the species (“others” in Fig. 4) shifted from
461 having a peak at the smaller end of the accumulation mode (0.18 – 0.32 μm) before and after the
462 firework event to larger sizes in the accumulation mode (0.56 – 1.0 μm) during the firework
463 event. The shift in mode to slightly larger particles during the firework event may be due to
464 increased coagulation sinks (Zhang et al., 2010) and secondary production (Retama et al., 2019).
465 An additional coarse peak (3.2 – 5.6 μm) observed after the firework event is mainly attributed
466 to sea salt constituents (e.g., Cl^- , Na^+) and likely unrelated to firework emissions aging and
467 processing. The mass contribution of the “others” to the total measured water-soluble mass
468 concentration decreased during the firework event to 4.3% from 12.5% before and 11.6% after
469 the firework event due to the prevalence of the ionic species (nss-SO_4^{2-} , K^+ , NO_3^- , Cl^- , Mg^{2+} , Na^+ ,
470 Ca^{2+} , and NH_4^+) discussed earlier (Table 1).

471

472 3.4 Enriched Tracers in Firework Emissions

473 Here we more closely examine how much concentrations of species changed during the firework
474 event. Bulk mass concentrations of eighteen of the forty-one measured species were enriched
475 during the firework event by more than two times compared to the average of their bulk mass
476 concentrations before and after the firework event (Fig. 5). Enrichments for Cu (65.2), Sr (24.4),
477 succinate (19.4), Ba (18.2), K^+ (16.3), nss-SO_4^{2-} (9.8), Al (6.9), Pb (6.1), and maleate (5.3) were
478 highest (> 5) among the species measured (Fig.5). Potassium and nss-SO_4^{2-} together contributed
479 to 70.9% of the total measured species during the firework event (Table 1). However, Cu, Sr,

480 succinate, Ba, Al, Pb, and maleate contributed a total of only 2.1% to the total measured species
481 mass concentration. This reinforces the importance of looking at enrichments rather than
482 absolute mass concentrations for identifying which aerosol constituents are firework tracers.
483 Tracer metals in firework emissions were previously shown to contribute a small fraction
484 ($\sim < 2\%$) to total PM mass (Jiang et al., 2014).

485 Of the eighteen species with observed enrichments exceeding two (Fig. 5), only those which are
486 firework components and that are uninfluenced by secondary formation are considered tracers.
487 The identified fourteen firework tracers based on these criteria are as follows: Cu, Sr, Ba, K^+ , Al,
488 Pb, Mg^{2+} , Cr, Tl, Cl^- , Mn, Rb, Zn, and Ag. Copper gives the blue-violet color of fireworks, Sr
489 gives the red color, Ba and Tl makes the green flame, and Rb gives a purple color. Potassium and
490 Ag (as AgCNO or silver fulminate) are propellants, Al is fuel, and Pb provides steady burn and
491 is also used as an igniter for firework explosions. Chromium is a catalyst for propellants, Mg is a
492 fuel, and Mg^{2+} is a neutralizer or oxygen donor (U.S. Department of Transportation, 2013).
493 Manganese is either a fuel or oxidizer, and Zn is used for sparks (Licudine et al., 2012; Martín-
494 Alberca and García-Ruiz, 2014; Shimizu, 1988; Wang et al., 2007; Ennis and Shanley, 1991).
495 Metals are usually in the form of Cl^- salts in fireworks (Wang et al., 2007). In this study, the
496 enrichment of Cl^- during the firework event was found to be 3.7. Some of the identified tracer
497 metals are regulated and their detection is of concern. Magnesium is not recommended as a
498 firework component because it is sensitive to heat and can easily ignite in storage (Do et al.,
499 2012). Lead is highly toxic and thus regulated (Moreno et al., 2010) as its occurrence in
500 fireworks is a serious health hazard. Although SO_4^{2-} , maleate (fuel), and NO_3^- (oxidant) were
501 also enriched more than two times during the firework event and are also firework components
502 (Zhang et al., 2019), they can be formed secondarily via gas-to-particle conversion processes
503 (Yang et al., 2014) and are not considered as firework tracers. Succinate is likewise formed
504 secondarily and is not considered a firework tracer (Wang et al., 2007). The identified firework
505 tracers with the highest enrichments (> 5) (excluding K^+), including Cu, Sr, Ba, Al, and Pb,
506 together contributed 2.1% to the total measured species mass concentration during the firework
507 event (Table 1).

508 Size-resolved enrichments (Fig. 6) were highest in the submicrometer range for most measured
509 species. This is consistent with past studies such as in Italy (Vecchi et al., 2008), Taiwan (Do et
510 al., 2012), and Spain (Crespo et al., 2012) where elemental concentrations due to pyrotechnics
511 increased in the submicrometer mode. The peak size differentiated enrichments of the first five
512 firework tracers Sr (45.08), Ba (57.82), K^+ (48.70), Al (18.75), and Pb (69.07) were in the 1.0 –
513 1.8 μm size range. Copper (49.85) peaked between 0.56 – 1.0 μm because it did not have valid
514 data for diameters exceeding 1.0 μm . Strontium and Ba had very high enrichments (254.40 and
515 195.84) from 0.1 – 0.18 μm due to very low concentrations before and after the firework event in
516 that size range. Enrichments of up to ~ 1000 (Crespo et al., 2012) for Sr and Ba have been
517 observed due to pyrotechnics, and both are known firework tracers (Kong et al., 2015).

518 The size-resolved enrichments of other notable species (Fig. 6 and Fig. S6) peaked at specific
519 size ranges between 0.32 – 1.8 μm : Mg^{2+} (18.93, 0.056 – 0.1 μm), Cr (14.37, 1.0 – 1.8 μm), Tl

520 (18.12, 0.56 – 1.0 μm), Cl^- (170.94, 0.32 – 0.56 μm), Mn (6.29, 1.0 – 1.8 μm), Rb (6.87, 1.0 –
521 1.8 μm), NO_3^- (7.26, 0.56 – 1.0 μm), Cs (6.28, 1.0 – 1.8 μm), Mo (4.15, 0.32 – 0.56 μm), Ti
522 (6.63, 0.32 – 0.56 μm), Co (17.94, 0.56 – 1.0 μm), and methanesulfonate (MSA) (6.66, 0.56 –
523 1.0 μm). Among all the measured water-soluble species, Cl^- had the highest size-resolved
524 enrichment, followed by Sr, Ba, K^+ , Pb, and Cu. This is expected because inorganic salts
525 comprise an enormous percentage of firework emissions (Martín-Alberca et al., 2016).

526

527 3.5 SEM-EDX

528 In addition to size-resolved species concentrations, the morphology of particles is important with
529 regard to their optical properties, hygroscopicity, and their transport behavior. Five SEM
530 images from the different stages (0.18 – 1 μm) of the MOUDI sampler with possible firework
531 influence are highlighted (Fig. 7). There were signs of nano-scale aggregation that were chain-
532 like and reminiscent of soot particles from pyrolysis and combustion (Pirker et al., 2020; Pósfai
533 et al., 2003; D’Anna, 2015) in all of the images, and especially distinct in the 0.1 – 0.18 μm (Fig.
534 4b) and 0.18 – 0.32 μm (Fig.7c) stages. Images for larger sizes revealed relatively larger particles
535 appearing as a translucent crystal-shaped rectangle in the 0.32 – 0.56 μm image (Fig. 7d), in
536 addition to a capsule-shaped particle (Fig. 7e) and a cubic-shaped particle (Fig. 7f) in the two
537 0.56 – 1.0 μm images. The presence of such non-spherical shapes including chain aggregates
538 points to the potential for particle collapse and shrinking associated with humidified conditions
539 as noted in past work (Shingler et al., 2016 and references therein).

540 The chemical composition of the blank Teflon substrate (Fig. 7a) was examined first by EDX to
541 determine the background signals before the actual samples were analyzed. The color intensity of
542 the element maps (Fig. S7) relates the concentration of the analyzed element relative to the
543 backscattered electron image (gray-scale) of the sample. The background substrate was
544 dominated by C, F, and Al (bright yellow, bright blue, and bright blue-green, respectively, in Fig.
545 S7-a1/a2/a3). Metallic elements were distributed in each of the five featured SEM images.
546 Molybdenum and K were present in all of the substrate stages (bright red in Fig. S7-
547 b3/b4/c3/c8/d7/d8/e6/e7/f6/f9). Other metals were also found in the different stages such as K,
548 Mg, Al, Ru, Pd, Ba, Hf, and Tl. The identified heavy metals in the particles are commonly used
549 in firework as fuel components, colorants, and oxidants (Singh et al., 2019). Potassium, Mg, Al,
550 Ba, and Tl are in the group of firework tracers that were already identified (Section 3.4 and Fig.
551 5) to have mass bulk concentration enrichments exceeding two. Molybdenum exhibited a
552 reduced mass bulk concentration enrichment of 1.93 (Fig. 5), but had size-resolved enrichments
553 between 1.21 and 4.15 (Fig. 6) in the substrate cut-outs analyzed for EDX. The cube-shaped
554 feature in the 0.56 – 1.0 μm substrate appears to be KCl because of the high color density of K
555 and Cl in the elemental maps (bright red and bright blue-green in Fig. S7-f6/f8) and because the
556 shape of KCl is cubic (Pirker et al., 2020). The crystal-shaped rectangle in the 0.32 – 0.56 μm
557 range appears to be enriched by Cl (bright blue-green in Fig. S7-d6). The same applies to the
558 capsule-shaped particle in 0.56 – 1.0 μm image (bright blue-green in Fig. S7-e5). The chloride

559 ion (Cl^-) is a component of metal salts, usually in the form of ClO_4^- or ClO_3^- (Tian et al., 2014)
560 used to color fireworks (Shimizu, 1988).

561 These results of the sampled portions of the substrate stages are consistent with the results of the
562 size-resolved submicrometer enrichments measured by IC and ICP-QQQ (Section 3.4) for Mo,
563 K, Mg, Al, Ba, and Tl. Molybdenum was brightest red in the $0.32 - 0.56 \mu\text{m}$ image (Fig. S7-d8),
564 consistent with the highest enrichments (4.15 in Fig. 6) for that size range. Potassium was
565 brightest red in the $0.56 - 1.0 \mu\text{m}$ image (Fig. S7-e6/f6), consistent with highest enrichments
566 (33.04 in Fig. 6). Magnesium was brightest yellow from $0.32 - 1.0 \mu\text{m}$ (Fig. S7-d4/e3/f4),
567 consistent with highest enrichments (9.50 and 11.58 in Fig. 6). Aluminum had a high signal in
568 the blank Teflon substrate but also was brightest blue-green (Fig. S7-d5/e4/f5) in between $0.32 -$
569 $1.0 \mu\text{m}$ in the sample during the firework event, consistent with highest enrichments (9.22 and
570 13.32 in Fig. 6). Barium was detected by EDX between $0.56 - 1.0 \mu\text{m}$ (Fig. S7-f11 where its
571 enrichment was 12.39 (Fig. 6). Thallium was detected between 0.56 and $1.0 \mu\text{m}$ (Fig. S7-f13) by
572 EDX, where its enrichment was highest (18.12 in Fig. 7) as detected by ICP-QQQ. The
573 submicrometer metal salts due to fireworks can uptake water at high humidity (ten Brink et al.,
574 2018).

575

576 3.6 Hygroscopicity Analysis

577 As fireworks alter the chemical profile of ambient PM, we estimate how aerosol hygroscopicity
578 responded during fireworks relative to periods before and after. For reference, typical κ values
579 range from 0.1 to 0.5 for diverse air mass types such as urban, marine, biogenic, biomass
580 burning, and free troposphere (Dusek et al., 2010; Hersey et al., 2013; Shingler et al., 2016;
581 Shinozuka et al., 2009). AzadiAghdam et al. (2019) reported size-resolved values ranging from
582 0.02 to 0.31 using data from the same field site in Metro Manila but for a different time period
583 and without any firework influence (July – December 2018). They found the highest values to be
584 coincident with MOUDI stages with most sea salt influence ($3.2 - 5.6 \mu\text{m}$).

585 For this study, a bulk κ value is reported for the size range between $0.056 - 3.2 \mu\text{m}$ as noted in
586 Section 2.7, and subsequent references to composition data are for this size range. Kappa was
587 enhanced during the firework event (0.18) compared to before (0.11), due mostly to increased
588 contributions from K_2SO_4 and $\text{Mg}(\text{NO}_3)_2$ (Fig. 8a). More specifically, the volume fractions of
589 K_2SO_4 and $\text{Mg}(\text{NO}_3)_2$ increased from 0.01 to 0.10 and 0.01 to 0.03, respectively (Fig. 8b).
590 Notable reductions in volume fraction during the firework event were for NaNO_3 (0.01 to 0.00),
591 black carbon (0.26 to 0.12), and $(\text{NH}_4)_2\text{SO}_4$ (0.02 to 0.01) (Fig. 8b). All three species are not
592 associated with primary firework emissions. Although NaNO_3 and $(\text{NH}_4)_2\text{SO}_4$ are hygroscopic,
593 their decreased volume fractions happened alongside a decreased volume fraction of non-
594 hygroscopic black carbon and increased volume fractions of the firework-related and
595 hygroscopic K_2SO_4 and $\text{Mg}(\text{NO}_3)_2$, which increased bulk aerosol hygroscopicity during the
596 firework event.

597 Kappa decreased to an intermediate value after the firework event (0.15) (Fig. 8a); this value
598 exceeds that from before the fireworks owing partly to more sea salt influence that was unrelated
599 to fireworks. The change in volume fraction of sea salt from before and during fireworks (0.01)
600 to after the fireworks (0.03) (Fig. 8b) translated to an increase of 0.03 in bulk κ (Fig. 8a) from
601 before to after the firework event. Although fireworks emit extensive amounts of inorganic
602 species, the calculated κ values were still relatively low because the background air is dominated
603 by organics and black carbon, which are relatively hydrophobic species (Table S4) (Cohen et al.,
604 2009; Oanh et al., 2006; Cruz et al., 2019).

605

606 4. Conclusion

607 This study reports on important aerosol characteristics measured during the 2019 New Year
608 fireworks in Metro Manila. Notable results of this work, following the order of questions raised
609 at the end of Section 1, are as follows:

- 610 • Firework activities caused significant enhancement of PM_{2.5} reaching a maximum of
611 383.9 $\mu\text{g m}^{-3}$ between 01:00 to 02:00 on 1 January 2019. Surface aerosol loading
612 increased over a period of eight hours during the firework event, coincident with peak
613 PM_{2.5} levels. The heaviest aerosol layer measured by the HSRL lidar was observed for at
614 least an hour, and reached ~440 m above the surface, after which the aerosol layer
615 dropped to 118 ± 20 m. Aerosol backscatter during the firework activity decreased
616 noticeably for short periods after rainfall. Besides rainfall, wind, and relative humidity
617 also possibly contributed to washout, local dispersion, and secondary formation of
618 particles, respectively. There was no significant influence from long-range transport to
619 the sampling site, confirming that the sample data was most representative of the local
620 nature of particulate enhancements observed during the firework event.
- 621 • The firework event enhanced bulk concentrations of water-soluble aerosol species,
622 especially in the submicrometer range. Mass size distributions of the water-soluble
623 species shifted to slightly larger accumulation-mode sizes most likely due to increased
624 coagulation sinks and secondary formation. Potassium and nss-SO₄²⁻ were the major
625 water-soluble contributors. Cubic and capsule-shaped Cl⁻-rich particles were prominent in
626 submicrometer particles collected during the firework event, suggesting the presence of
627 KCl. Inorganic species including Cu, Sr, Ba, K⁺, Al, Pb, Mg²⁺, Cr, Tl, Cl⁻, Mn, Rb, Zn,
628 and Ag were enriched more than two times by mass during the firework event as
629 compared to before and after the event. While the most enriched inorganic firework
630 tracers, including Cu, Sr, Ba, Al, and Pb (excluding K⁺), comprised only 2.1% of the total
631 water-soluble mass, their contribution is significant because they support findings that the
632 samples represent firework emissions. The increased volume fractions of inorganics
633 increased aerosol hygroscopicity (κ) between 0.056 and 3.2 μm from 0.11 (before the
634 fireworks) to 0.18 during the firework event.

635 Fireworks caused unhealthy levels of PM_{2.5} that exceeded the Philippine (50.0 μg m⁻³), U.S.
636 (35.0 μg m⁻³), and World Health Organization (WHO, 25.0 μg m⁻³) standards for PM_{2.5} over 24
637 hours. The brief but sharply enhanced concentrations of water-soluble species in the
638 submicrometer size range, especially for K⁺ and SO₄²⁻, have implications for both public health
639 and the environment, the former of which is owing to how smaller particles can penetrate more
640 deeply into the human respiratory system. Some of the components detected during the fireworks
641 were submicrometer Pb and Mg²⁺, which is of concern because these are banned substances due
642 to their being health and fire hazards, respectively. The presence of Pb in the firework emissions
643 exacerbates the presence of submicrometer Pb in Metro Manila (Gonzalez et al., 2021). The
644 results show the opportunity that improved quality and management of fireworks can have for
645 better local air quality.

646 Higher concentrations of secondary particles in the accumulation mode from fireworks are
647 related to increased mass extinction efficiency and therefore decreased visibility (Jiang et al.,
648 2014), as was observed in this study. The increased water-soluble fraction, especially in the
649 submicrometer mode, during firework events coincides with elevated particle hygroscopicity,
650 which is related to CCN activity (Drewnick et al., 2006) at smaller diameters (Yuan et al., 2020),
651 with implications that can be better assessed in a future study. The atmospheric environment in
652 Southeast Asia, coupled with increasing emissions and extreme sources such as fireworks, offers
653 a unique field laboratory for the study of aerosol aqueous processes.

654

655 **Data availability**

656 High Spectral Resolution Lidar data collected at Manila Observatory can be found at:
657 (University of Wisconsin Lidar Group) http://hsrl.ssec.wisc.edu/by_site/30/custom_rti/

658 Size-resolved aerosols data collected at Manila Observatory can be found at: (Stahl et al., 2020a)
659 on figshare as well as on the NASA data repository at
660 DOI:10.5067/Suborbital/CAMP2EX2018/DATA001.

661

662 **Author Contributions**

663 MTC, MOC, JBS, RAB, ABM, CS, and AS designed the experiments. All coauthors carried out
664 various aspects of the data collection. MTC, EE, SV, RH, GL, LM, CS, and AS conducted
665 analysis and interpretation of the data. EE, LM, SV, RH, GL, and AS prepared the manuscript
666 with contributions from the coauthors.

667

668 **Competing Interests**

669 The authors declare that they have no conflict of interest.

670

671 **Acknowledgements**

672 The authors acknowledge support from NASA grant 80NSSC18K0148 in support of the NASA
673 CAMP²Ex project. R. A. Braun acknowledges support from the ARCS Foundation. M. T. Cruz
674 acknowledges support from the Philippine Department of Science and Technology's ASTHRD
675 Program. A. B. MacDonald acknowledges support from the Mexican National Council for
676 Science and Technology (CONACYT). We acknowledge Agilent Technologies for their support
677 and Shane Snyder's laboratories for ICP-QQQ data. We thank the Department of Environment
678 and Natural Resources Environmental Management Bureau (DENR-EMB) Central Office Air
679 Quality Management Section in the Philippines and the Air Center for Air Pollution Research in
680 Japan of EANET for the hourly PM_{2.5} data. The tradition of sampling the New Year air quality in
681 Metro Manila was instilled by Fr. Dan McNamara, SJ, Fr. Jett Villarin, SJ, and Gemma Narisma,
682 and for this we are grateful.

683

684 **References**

685 Agus, E. L., Lingard, J. J., and Tomlin, A. S.: Suppression of nucleation mode particles by
686 biomass burning in an urban environment: a case study, *Journal of Environmental Monitoring*,
687 10, 979-988, 2008.

688 Aldhaif, A. M., Lopez, D. H., Dadashazar, H., and Sorooshian, A.: Sources, frequency, and
689 chemical nature of dust events impacting the United States East Coast, *Atmospheric*
690 *Environment*, 117456, 2020.

691 Alpert, D. J., and Hopke, P. K.: A determination of the sources of airborne particles collected
692 during the regional air pollution study, *Atmospheric Environment* (1967), 15, 675-687, 1981.

693 Arimoto, R., Duce, R., Savoie, D., Prospero, J., Talbot, R., Cullen, J., Tomza, U., Lewis, N., and
694 Ray, B.: Relationships among aerosol constituents from Asia and the North Pacific during PEM-
695 West A, *Journal of Geophysical Research: Atmospheres*, 101, 2011-2023, 1996.

696 AzadiAghdam, M., Braun, R. A., Edwards, E.-L., Bañaga, P. A., Cruz, M. T., Betito, G.,
697 Cambaliza, M. O., Dadashazar, H., Lorenzo, G. R., and Ma, L.: On the nature of sea salt aerosol
698 at a coastal megacity: Insights from Manila, Philippines in Southeast Asia, *Atmospheric*
699 *Environment*, 216, 116922, 2019.

700 Barman, S., Singh, R., Negi, M., and Bhargava, S.: Ambient air quality of Lucknow City (India)
701 during use of fireworks on Diwali Festival, *Environmental monitoring and assessment*, 137, 495-
702 504, 2008.

703 Becker, J. M., Iskandrian, S., and Conkling, J.: Fatal and near-fatal asthma in children exposed to
704 fireworks, *Annals of Allergy, Asthma & Immunology*, 85, 512-513, 2000.

705 Beig, G., Chate, D., Ghude, S. D., Ali, K., Satpute, T., Sahu, S., Parkhi, N., and Trimbake, H.:
706 Evaluating population exposure to environmental pollutants during Deepavali fireworks displays
707 using air quality measurements of the SAFAR network, *Chemosphere*, 92, 116-124, 2013.

708 Braun, R. A., Dadashazar, H., MacDonald, A. B., Aldhaif, A. M., Maudlin, L. C., Crosbie, E.,
709 Aghdam, M. A., Hossein Mardi, A., and Sorooshian, A.: Impact of wildfire emissions on
710 chloride and bromide depletion in marine aerosol particles, *Environmental Science &*
711 *Technology*, 51, 9013-9021, 2017.

712 Braun, R. A., Aghdam, M. A., Bañaga, P. A., Betito, G., Cambaliza, M. O., Cruz, M. T.,
713 Lorenzo, G. R., MacDonald, A. B., Simpas, J. B., and Stahl, C.: Long-range aerosol transport
714 and impacts on size-resolved aerosol composition in Metro Manila, Philippines, *Atmospheric*
715 *Chemistry and Physics*, 20, 2387-2405, 2020.

716 Cao, Y., Zhang, Z., Xiao, H., Xie, Y., Liang, Y., and Xiao, H.: How aerosol pH responds to
717 nitrate to sulfate ratio of fine-mode particulate, *Environmental Science and Pollution Research*,
718 1-9, 2020.

719 Carranza, J., Fisher, B., Yoder, G., and Hahn, D.: On-line analysis of ambient air aerosols using
720 laser-induced breakdown spectroscopy, *Spectrochimica Acta Part B: Atomic spectroscopy*, 56,
721 851-864, 2001.

722 Chatterjee, A., Sarkar, C., Adak, A., Mukherjee, U., Ghosh, S., and Raha, S.: Ambient air quality
723 during Diwali Festival over Kolkata-a mega-city in India, *Aerosol and Air Quality Research*, 13,
724 1133-1144, 2013.

725 Cheng, Y., Engling, G., He, K.-b., Duan, F.-k., Du, Z.-y., Ma, Y.-l., Liang, L.-l., Lu, Z.-f., Liu,
726 J.-m., and Zheng, M.: The characteristics of Beijing aerosol during two distinct episodes:
727 Impacts of biomass burning and fireworks, *Environmental Pollution*, 185, 149-157, 2014.

728 Cohen, D. D., Stelcer, E., Santos, F. L., Prior, M., Thompson, C., and Pabroa, P. C.:
729 Fingerprinting and source apportionment of fine particle pollution in Manila by IBA and PMF
730 techniques: A 7-year study, *X-Ray Spectrometry: An International Journal*, 38, 18-25, 2009.

731 Crespo, J., Yubero, E., Nicolás, J. F., Lucarelli, F., Nava, S., Chiari, M., and Calzolari, G.: High-
732 time resolution and size-segregated elemental composition in high-intensity pyrotechnic
733 exposures, *Journal of hazardous materials*, 241, 82-91, 2012.

734 Crosbie, E., Sorooshian, A., Monfared, N. A., Shingler, T., and Esmaili, O.: A multi-year aerosol
735 characterization for the greater Tehran area using satellite, surface, and modeling data,
736 *Atmosphere*, 5, 178-197, 2014.

737 Cruz, M. T., Bañaga, P. A., Betito, G., Braun, R. A., Stahl, C., Aghdam, M. A., Cambaliza, M.
738 O., Dadashazar, H., Hilario, M. R., and Lorenzo, G. R.: Size-resolved composition and
739 morphology of particulate matter during the southwest monsoon in Metro Manila, Philippines,
740 2019.

741 D'Anna, A.: *Kinetics of Soot Formation*, 2015.

742 de Leeuw, G., Cohen, L., Frohn, L. M., Geernaert, G., Hertel, O., Jensen, B., Jickells, T., Klein,
743 L., Kunz, G. J., and Lund, S.: Atmospheric input of nitrogen into the North Sea: ANICE project
744 overview, *Continental Shelf Research*, 21, 2073-2094, 2001.

745 Devara, P. C., Vijayakumar, K., Safai, P. D., Made, P. R., and Rao, P. S.: Celebration-induced
746 air quality over a tropical urban station, Pune, India, *Atmospheric Pollution Research*, 6, 511-
747 520, 2015.

748 Do, T.-M., Wang, C.-F., Hsieh, Y.-K., and Hsieh, H.-F.: Metals present in ambient air before and
749 after a firework festival in Yanshui, Tainan, Taiwan, *Aerosol and Air Quality Research*, 12, 981-
750 993, 2012.

751 Dorado, S. V., Holdsworth, J. L., Lagrosas, N. C., Villarin, J. R., Narisma, G., Ellis, J., and
752 Perez, R.: Characterization of urban atmosphere of Manila with lidar, filter sampling, and
753 radiosonde, *Lidar Remote Sensing for Industry and Environment Monitoring*, 2001, 591-598,

754 Drewnick, F., Hings, S. S., Curtius, J., Eerdekens, G., and Williams, J.: Measurement of fine
755 particulate and gas-phase species during the New Year's fireworks 2005 in Mainz, Germany,
756 *Atmospheric Environment*, 40, 4316-4327, 2006.

757 Dusek, U., Frank, G., Curtius, J., Drewnick, F., Schneider, J., Kürten, A., Rose, D., Andreae, M.
758 O., Borrmann, S., and Pöschl, U.: Enhanced organic mass fraction and decreased hygroscopicity
759 of cloud condensation nuclei (CCN) during new particle formation events, *Geophysical Research*
760 *Letters*, 37, 2010.

761 Dutcher, D. D., Perry, K. D., Cahill, T. A., and Copeland, S. A.: Effects of indoor pyrotechnic
762 displays on the air quality in the Houston Astrodome, *Journal of the Air & Waste Management*
763 *Association*, 49, 156-160, 1999.

764 Ennis, J. L., and Shanley, E. S.: On hazardous silver compounds, *Journal of Chemical Education*,
765 68, A6, 1991.

766 Feng, J., Sun, P., Hu, X., Zhao, W., Wu, M., and Fu, J.: The chemical composition and sources
767 of PM_{2.5} during the 2009 Chinese New Year's holiday in Shanghai, *Atmospheric Research*,
768 118, 435-444, 2012.

769 Gonzalez, M. E., Stahl, C., Cruz, M. T., Bañaga, P. A., Betito, G., Braun, R. A., Aghdam, M. A.,
770 Cambaliza, M. O., Lorenzo, G. R., and MacDonald, A. B.: Contrasting the size-resolved nature
771 of particulate arsenic, cadmium, and lead among diverse regions, *Atmospheric Pollution*
772 *Research*, 2021.

773 Gysel, M., Crosier, J., Topping, D., Whitehead, J., Bower, K., Cubison, M., Williams, P., Flynn,
774 M., McFiggans, G., and Coe, H.: Closure study between chemical composition and hygroscopic
775 growth of aerosol particles during TORCH2, 2007.

776 Hersey, S. P., Craven, J. S., Metcalf, A. R., Lin, J., Latham, T., Suski, K. J., Cahill, J. F., Duong,
777 H. T., Sorooshian, A., and Jonsson, H. H.: Composition and hygroscopicity of the Los Angeles
778 aerosol: CalNex, *Journal of Geophysical Research: Atmospheres*, 118, 3016-3036, 2013.

779 Hilario, M. R. A., Cruz, M. T., Bañaga, P. A., Betito, G., Braun, R. A., Stahl, C., Cambaliza, M.
780 O., Lorenzo, G. R., MacDonald, A. B., and AzadiAghdam, M.: Characterizing weekly cycles of
781 particulate matter in a coastal megacity: The importance of a seasonal, size-resolved, and
782 chemically-specified analysis, *Journal of Geophysical Research: Atmospheres*, e2020JD032614,
783 2020.

784 Hirai, K., Yamazaki, Y., Okada, K., FURUTA, S., and KUBO, K.: Acute eosinophilic
785 pneumonia associated with smoke from fireworks, *Internal medicine*, 39, 401-403, 2000.

786 Hooper, W. P., and Eloranta, E. W.: Lidar measurements of wind in the planetary boundary
787 layer: the method, accuracy and results from joint measurements with radiosonde and kytoon,
788 *Journal of climate and applied meteorology*, 25, 990-1001, 1986.

789 Hopke, P. K., Cohen, D. D., Begum, B. A., Biswas, S. K., Ni, B., Pandit, G. G., Santoso, M.,
790 Chung, Y.-S., Davy, P., and Markwitz, A.: Urban air quality in the Asian region, *Science of the*
791 *Total Environment*, 404, 103-112, 2008.

792 Hussein, T., Dal Maso, M., Petaja, T., Koponen, I. K., Paatero, P., Aalto, P. P., Hameri, K., and
793 Kulmala, M.: Evaluation of an automatic algorithm for fitting the particle number size
794 distributions, *Boreal environment research*, 10, 337, 2005.

795 Jiang, Q., Sun, Y., Wang, Z., and Yin, Y.: Aerosol composition and sources during the Chinese
796 Spring Festival: fireworks, secondary aerosol, and holiday effects, *ACPD*, 14, 20617-20646,
797 2014.

798 Joly, A., Smargiassi, A., Kosatsky, T., Fournier, M., Dabek-Zlotorzynska, E., Celo, V., Mathieu,
799 D., Servranckx, R., D'amours, R., and Malo, A.: Characterisation of particulate exposure during
800 fireworks displays, *Atmospheric Environment*, 44, 4325-4329, 2010.

801 Joshi, M., Khan, A., Anand, S., and Sapra, B.: Size evolution of ultrafine particles: Differential
802 signatures of normal and episodic events, *Environmental pollution*, 208, 354-360, 2016.

803 Joshi, M., Nakhwa, A., Khandare, P., Khan, A., and Sapra, B.: Simultaneous measurements of
804 mass, chemical compositional and number characteristics of aerosol particles emitted during
805 fireworks, *Atmospheric Environment*, 217, 116925, 2019.

806 Karnae, S.: Analysis of aerosol composition and characteristics in a semi arid coastal urban area,
807 Texas A&M University-Kingsville, 2005.

808 Khaparde, V. V., Pipalatkhar, P. P., Pustode, T., Rao, C. C., and Gajghate, D. G.: Influence of
809 burning of fireworks on particle size distribution of PM 10 and associated barium at Nagpur,
810 Environmental monitoring and assessment, 184, 903-911, 2012.

811 Kong, S., Li, L., Li, X., Yin, Y., Chen, K., Liu, D., Yuan, L., Zhang, Y., Shan, Y., and Ji, Y.: The
812 impacts of firework burning at the Chinese Spring Festival on air quality: insights of tracers,
813 source evolution and aging processes, *Atmos. Chem. Phys.*, 15, 2167-2184, 2015.

814 Kulshrestha, U., Rao, T. N., Azhaguvel, S., and Kulshrestha, M.: Emissions and accumulation of
815 metals in the atmosphere due to crackers and sparkles during Diwali festival in India,
816 *Atmospheric Environment*, 38, 4421-4425, 2004.

817 Kumar, M., Singh, R., Murari, V., Singh, A., Singh, R., and Banerjee, T.: Fireworks induced
818 particle pollution: a spatio-temporal analysis, *Atmospheric research*, 180, 78-91, 2016.

819 Lai, Y., and Brimblecombe, P.: Changes in air pollution and attitude to fireworks in Beijing,
820 *Atmospheric Environment*, 117549, 2020.

821 Li, J., Xu, T., Lu, X., Chen, H., Nizkorodov, S. A., Chen, J., Yang, X., Mo, Z., Chen, Z., and
822 Liu, H.: Online single particle measurement of fireworks pollution during Chinese New Year in
823 Nanning, *Journal of Environmental Sciences*, 53, 184-195, 2017.

824 Licudine, J. A., Yee, H., Chang, W. L., and Whelen, A. C.: Hazardous metals in ambient air due
825 to New Year fireworks during 2004–2011 celebrations in Pearl City, Hawaii, *Public Health*
826 *Reports*, 127, 440-450, 2012.

827 Lin, C.-C.: A review of the impact of fireworks on particulate matter in ambient air, *Journal of*
828 *the Air & Waste Management Association*, 66, 1171-1182, 2016.

829 Lin, C.-C., Yang, L.-S., and Cheng, Y.-H.: Ambient PM_{2.5}, black carbon, and particle size-
830 resolved number concentrations and the Ångström exponent value of aerosols during the
831 firework display at the lantern festival in southern Taiwan, *Aerosol Air Qual. Res.*, 16, 373-387,
832 2016.

833 Liu, D.-Y., Rutherford, D., Kinsey, M., and Prather, K. A.: Real-time monitoring of
834 pyrotechnically derived aerosol particles in the troposphere, *Analytical Chemistry*, 69, 1808-
835 1814, 1997.

836 Marple, V., Olson, B., Romay, F., Hudak, G., Geerts, S. M., and Lundgren, D.: Second
837 generation micro-orifice uniform deposit impactor, 120 MOUDI-II: Design, evaluation, and
838 application to long-term ambient sampling, *Aerosol Science and Technology*, 48, 427-433, 2014.

839 Martín-Alberca, C., and García-Ruiz, C.: Analytical techniques for the analysis of consumer
840 fireworks, *TrAC Trends in Analytical Chemistry*, 56, 27-36, 2014.

841 Martín-Alberca, C., Zapata, F., Carrascosa, H., Ortega-Ojeda, F. E., and García-Ruiz, C.: Study
842 of consumer fireworks post-blast residues by ATR-FTIR, *Talanta*, 149, 257-265, 2016.

843 Mönkkönen, P., Uma, R., Srinivasan, D., Koponen, I., Lehtinen, K., Hämeri, K., Suresh, R.,
844 Sharma, V., and Kulmala, M.: Relationship and variations of aerosol number and PM10 mass
845 concentrations in a highly polluted urban environment—New Delhi, India, *Atmospheric*
846 *Environment*, 38, 425-433, 2004.

847 Mora, M., Braun, R. A., Shingler, T., and Sorooshian, A.: Analysis of remotely sensed and
848 surface data of aerosols and meteorology for the Mexico Megalopolis Area between 2003 and
849 2015, *Journal of Geophysical Research: Atmospheres*, 122, 8705-8723, 2017.

850 Moreno, T., Querol, X., Alastuey, A., Amato, F., Pey, J., Pandolfi, M., Kuenzli, N., Bouso, L.,
851 Rivera, M., and Gibbons, W.: Effect of fireworks events on urban background trace metal
852 aerosol concentrations: is the cocktail worth the show?, *Journal of hazardous materials*, 183, 945-
853 949, 2010.

854 Nicolás, J., Yubero, E., Galindo, N., Giménez, J., Castañer, R., Carratalá, A., Crespo, J., and
855 Pastor, C.: Characterization of events by aerosol mass size distributions, *Journal of*
856 *Environmental Monitoring*, 11, 394-399, 2009.

857 Oanh, N. K., Upadhyay, N., Zhuang, Y.-H., Hao, Z.-P., Murthy, D., Lestari, P., Villarín, J.,
858 Chengchua, K., Co, H., and Dung, N.: Particulate air pollution in six Asian cities: Spatial and
859 temporal distributions, and associated sources, *Atmospheric environment*, 40, 3367-3380, 2006.

860 Perrino, C., Tiwari, S., Catrambone, M., Dalla Torre, S., Rantica, E., and Canepari, S.: Chemical
861 characterization of atmospheric PM in Delhi, India, during different periods of the year including
862 Diwali festival, *Atmospheric Pollution Research*, 2, 418-427, 2011.

863 Perry, K. D.: Effects of outdoor pyrotechnic displays on the regional air quality of Western
864 Washington State, *Journal of the Air & Waste Management Association*, 49, 146-155, 1999.

865 Petters, M., and Kreidenweis, S.: A single parameter representation of hygroscopic growth and
866 cloud condensation nucleus activity, *Atmospheric Chemistry and Physics*, 7, 1961-1971, 2007.

867 Pirker, L., Gradišek, A., Višić, B., and Remškar, M.: Nanoparticle exposure due to pyrotechnics
868 during a football match, *Atmospheric Environment*, 117567, 2020.

869 Pósfai, M., Simonics, R., Li, J., Hobbs, P. V., and Buseck, P. R.: Individual aerosol particles
870 from biomass burning in southern Africa: 1. Compositions and size distributions of carbonaceous
871 particles, *Journal of Geophysical Research: Atmospheres*, 108, 2003.

872 Prospero, J. M., Savoie, D. L., and Arimoto, R.: Long-term record of nss-sulfate and nitrate in
873 aerosols on Midway Island, 1981–2000: Evidence of increased (now decreasing?) anthropogenic
874 emissions from Asia, *Journal of Geophysical Research: Atmospheres*, 108, AAC 10-11-AAC 10-
875 11, 2003.

876 Rao, P. S., Gajghate, D., Gavane, A., Suryawanshi, P., Chauhan, C., Mishra, S., Gupta, N., Rao,
877 C., and Wate, S.: Air quality status during Diwali Festival of India: A case study, *Bulletin of*
878 *environmental contamination and toxicology*, 89, 376-379, 2012.

879 Ravindra, K., Mor, S., and Kaushik, C.: Short-term variation in air quality associated with
880 firework events: a case study, *Journal of Environmental Monitoring*, 5, 260-264, 2003.

881 Razenkov, I.: Characterization of a Geiger-mode avalanche photodiode detector for high spectral
882 resolution lidar, University of Wisconsin--Madison, 2010.

883 Reid, J. S., Hyer, E. J., Johnson, R. S., Holben, B. N., Yokelson, R. J., Zhang, J., Campbell, J. R.,
884 Christopher, S. A., Di Girolamo, L., and Giglio, L.: Observing and understanding the Southeast
885 Asian aerosol system by remote sensing: An initial review and analysis for the Seven Southeast
886 Asian Studies (7SEAS) program, *Atmospheric Research*, 122, 403-468, 2013.

887 Retama, A., Neria-Hernández, A., Jaimes-Palomera, M., Rivera-Hernández, O., Sánchez-
888 Rodríguez, M., López-Medina, A., and Velasco, E.: Fireworks: a major source of inorganic and

889 organic aerosols during Christmas and New Year in Mexico city, *Atmospheric Environment*: X,
890 2, 100013, 2019.

891 Rolph, G., Stein, A., and Stunder, B.: Real-time environmental applications and display system:
892 READY, *Environmental Modelling & Software*, 95, 210-228, 2017.

893 Santos, F. L., Pabroa, P. C. B., Morco, R. P., and Racho, J. M. D.: Elemental characterization of
894 New Year's Day PM₁₀ and PM_{2.5} particulates matter at several sites in Metro Manila, *Book of*
895 *abstracts*, 2007,

896 Sarkar, S., Khillare, P. S., Jyethi, D. S., Hasan, A., and Parween, M.: Chemical speciation of
897 respirable suspended particulate matter during a major firework festival in India, *Journal of*
898 *Hazardous Materials*, 184, 321-330, 2010.

899 Schlosser, J. S., Braun, R. A., Bradley, T., Dadashazar, H., MacDonald, A. B., Aldhaif, A. A.,
900 Aghdam, M. A., Mardi, A. H., Xian, P., and Sorooshian, A.: Analysis of aerosol composition
901 data for western United States wildfires between 2005 and 2015: Dust emissions, chloride
902 depletion, and most enhanced aerosol constituents, *Journal of Geophysical Research*:
903 *Atmospheres*, 122, 8951-8966, 2017.

904 Shen, Z., Cao, J., Arimoto, R., Han, Z., Zhang, R., Han, Y., Liu, S., Okuda, T., Nakao, S., and
905 Tanaka, S.: Ionic composition of TSP and PM_{2.5} during dust storms and air pollution episodes
906 at Xi'an, China, *Atmospheric Environment*, 43, 2911-2918, 2009.

907 Shimizu, T.: *Fireworks: the art, science, and technique*, Pyrotechnica publications, 1988.

908 Shingler, T., Crosbie, E., Ortega, A., Shiraiwa, M., Zuend, A., Beyersdorf, A., Ziemba, L.,
909 Anderson, B., Thornhill, L., and Perring, A. E.: Airborne characterization of subsaturated aerosol
910 hygroscopicity and dry refractive index from the surface to 6.5 km during the SEAC4RS
911 campaign, *Journal of Geophysical Research: Atmospheres*, 121, 4188-4210, 2016.

912 Shinozuka, Y., Clarke, A., DeCarlo, P., Jimenez, J., Dunlea, E., Roberts, G., Tomlinson, J.,
913 Collins, D., Howell, S., and Kapustin, V.: Aerosol optical properties relevant to regional remote
914 sensing of CCN activity and links to their organic mass fraction: airborne observations over
915 Central Mexico and the US West Coast during MILAGRO/INTEX-B, 1foldr Import 2019-10-08
916 Batch 9, 2009.

917 Singh, A., Pant, P., and Pope, F. D.: Air quality during and after festivals: Aerosol
918 concentrations, composition and health effects, *Atmospheric Research*, 2019.

919 Stahl, C., Cruz, M. T., Bañaga, P. A., Betito, G., Braun, R. A., Aghdam, M. A., Cambaliza, M.
920 O., Lorenzo, G. R., MacDonald, A. B., Pabroa, P. C., Yee, J. R., Simpas, J. B., and Sorooshian,
921 A.: An annual time series of weekly size-resolved aerosol properties in the megacity of Metro
922 Manila, Philippines, *Scientific Data*, 7, 128, 10.1038/s41597-020-0466-y, 2020b.

923 Stein, A., Draxler, R. R., Rolph, G. D., Stunder, B. J., Cohen, M., and Ngan, F.: NOAA's
924 HYSPLIT atmospheric transport and dispersion modeling system, *Bulletin of the American*
925 *Meteorological Society*, 96, 2059-2077, 2015.

926 Steinhauser, G., and Klapotke, T. M.: Using the chemistry of fireworks to engage students in
927 learning basic chemical principles: a lesson in eco-friendly pyrotechnics, *Journal of Chemical*
928 *Education*, 87, 150-156, 2010.

929 Stokes, R., and Robinson, R.: Interactions in aqueous nonelectrolyte solutions. I. Solute-solvent
930 equilibria, *The Journal of Physical Chemistry*, 70, 2126-2131, 1966.

931 Sun, Y., Wang, Z., Fu, P., Jiang, Q., Yang, T., Li, J., and Ge, X.: The impact of relative humidity
932 on aerosol composition and evolution processes during wintertime in Beijing, China,
933 *Atmospheric Environment*, 77, 927-934, 2013.

934 Tanda, S., Ličbinský, R., Hegrová, J., and Goessler, W.: Impact of New Year's Eve fireworks on
935 the size resolved element distributions in airborne particles, *Environment international*, 128, 371-
936 378, 2019.

937 ten Brink, H., Henzing, B., Otjes, R., and Weijers, E.: Visibility in the Netherlands during New
938 Year's fireworks: The role of soot and salty aerosol products, *Atmospheric Environment*, 173,
939 289-294, 2018.

940 Thakur, B., Chakraborty, S., Debsarkar, A., Chakrabarty, S., and Srivastava, R.: Air pollution
941 from fireworks during festival of lights (Deepawali) in Howrah, India-a case study, *Atmosfera*,
942 23, 347-365, 2010.

943 Tian, Y., Wang, J., Peng, X., Shi, G., and Feng, Y.: Estimation of the direct and indirect impacts
944 of fireworks on the physicochemical characteristics of atmospheric PM10 and PM2. 5,
945 *Atmospheric Chemistry and Physics*, 9469, 2014.

946 Totsuka, T., Sase, H., and Shimizu, H.: Major activities of acid deposition monitoring network in
947 East Asia (EANET) and related studies, in: *Plant Responses to Air Pollution and Global Change*,
948 Springer, 251-259, 2005.

949 Tsai, H.-H., Chien, L.-H., Yuan, C.-S., Lin, Y.-C., Jen, Y.-H., and Ie, I.-R.: Influences of
950 fireworks on chemical characteristics of atmospheric fine and coarse particles during Taiwan's
951 Lantern Festival, *Atmospheric Environment*, 62, 256-264, 2012.

952 Tsai, J.-H., Lin, J.-H., Yao, Y.-C., and Chiang, H.-L.: Size distribution and water soluble ions of
953 ambient particulate matter on episode and non-episode days in Southern Taiwan, *Aerosol and*
954 *Air Quality Research*, 12, 263-274, 2011.

955 Tsay, S.-C., Hsu, N. C., Lau, W. K.-M., Li, C., Gabriel, P. M., Ji, Q., Holben, B. N., Welton, E.
956 J., Nguyen, A. X., and Janjai, S.: From BASE-ASIA toward 7-SEAS: A satellite-surface
957 perspective of boreal spring biomass-burning aerosols and clouds in Southeast Asia,
958 *Atmospheric environment*, 78, 20-34, 2013.

959 Vecchi, R., Bernardoni, V., Cricchio, D., D'Alessandro, A., Fermo, P., Lucarelli, F., Nava, S.,
960 Piazzalunga, A., and Valli, G.: The impact of fireworks on airborne particles, *Atmospheric*
961 *Environment*, 42, 1121-1132, 2008.

962 Villafuerte II, M. Q., Matsumoto, J., Akasaka, I., Takahashi, H. G., Kubota, H., and Cinco, T. A.:
963 Long-term trends and variability of rainfall extremes in the Philippines, *Atmospheric Research*,
964 137, 1-13, 2014.

965 Walsh, K. J., Milligan, M., and Sherwell, J.: Synoptic evaluation of regional PM2. 5
966 concentrations, *Atmospheric Environment*, 43, 594-603, 2009.

967 Wang, Y., Zhuang, G., Xu, C., and An, Z.: The air pollution caused by the burning of fireworks
968 during the lantern festival in Beijing, *Atmospheric Environment*, 41, 417-431, 2007.

969 Wehner, B., Wiedensohler, A., and Heintzenberg, J.: Submicrometer aerosol size distributions
970 and mass concentration of the millennium fireworks 2000 in Leipzig, Germany, *Journal of*
971 *Aerosol Science*, 12, 1489-1493, 2000.

972 Wilkin, R. T., Fine, D. D., and Burnett, N. G.: Perchlorate behavior in a municipal lake
973 following fireworks displays, *Environmental Science & Technology*, 41, 3966-3971, 2007.

974 Wonaschuetz, A., Sorooshian, A., Ervens, B., Chuang, P. Y., Feingold, G., Murphy, S. M., De
975 Gouw, J., Warneke, C., and Jonsson, H. H.: Aerosol and gas re-distribution by shallow cumulus
976 clouds: An investigation using airborne measurements, *Journal of Geophysical Research:*
977 *Atmospheres*, 117, 2012.

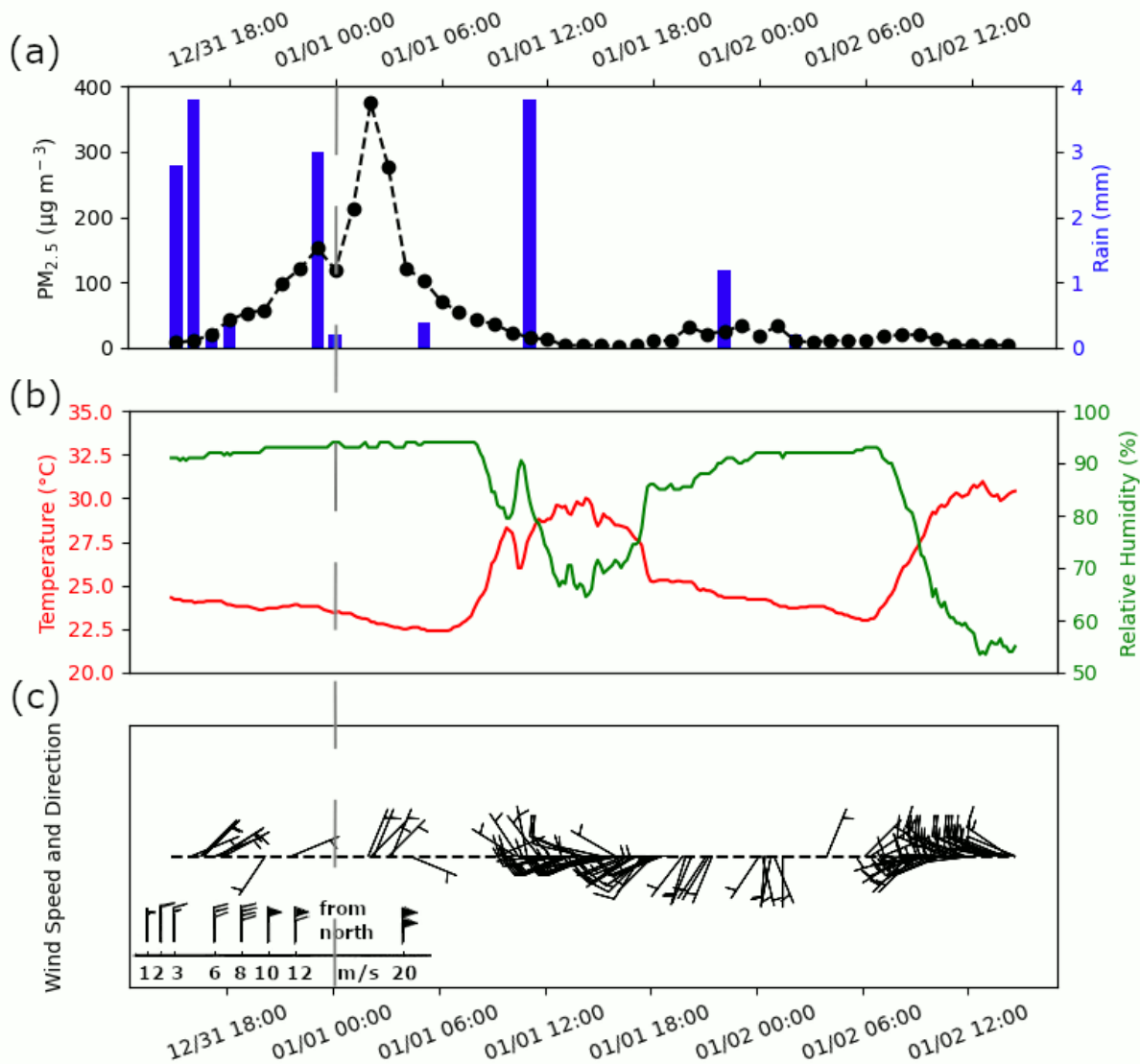
978 Wu, C., Wang, G., Wang, J., Li, J., Ren, Y., Zhang, L., Cao, C., Li, J., Ge, S., and Xie, Y.:
979 Chemical characteristics of haze particles in Xi'an during Chinese Spring Festival: Impact of
980 fireworks burning, *Journal of Environmental Sciences*, 71, 179-187, 2018.
981 Yadav, S. K., Kumar, M., Sharma, Y., Shukla, P., Singh, R. S., and Banerjee, T.: Temporal
982 evolution of submicron particles during extreme fireworks, *Environmental monitoring and*
983 *assessment*, 191, 576, 2019.
984 Yang, L., Gao, X., Wang, X., Nie, W., Wang, J., Gao, R., Xu, P., Shou, Y., Zhang, Q., and
985 Wang, W.: Impacts of firecracker burning on aerosol chemical characteristics and human health
986 risk levels during the Chinese New Year Celebration in Jinan, China, *Science of the Total*
987 *Environment*, 476, 57-64, 2014.
988 Youn, J. S., Wang, Z., Wonaschütz, A., Arellano, A., Betterton, E. A., and Sorooshian, A.:
989 Evidence of aqueous secondary organic aerosol formation from biogenic emissions in the North
990 American Sonoran Desert, *Geophysical research letters*, 40, 3468-3472, 2013.
991 Yuan, L., Zhang, X., Feng, M., Liu, X., Che, Y., Xu, H., Schaefer, K., Wang, S., and Zhou, Y.:
992 Size-resolved hygroscopic behaviour and mixing state of submicron aerosols in a megacity of the
993 Sichuan Basin during pollution and fireworks episodes, *Atmospheric Environment*, 226, 117393,
994 2020.
995 Zhang, J., Yang, L., Chen, J., Mellouki, A., Jiang, P., Gao, Y., Li, Y., Yang, Y., and Wang, W.:
996 Influence of fireworks displays on the chemical characteristics of PM_{2.5} in rural and suburban
997 areas in Central and East China, *Science of the Total Environment*, 578, 476-484, 2017.
998 Zhang, J., Lance, S., Freedman, J. M., Sun, Y., Crandall, B. A., Wei, X., and Schwab, J. J.:
999 Detailed Measurements of Submicron Particles from an Independence Day Fireworks Event in
1000 Albany, New York Using HR-ToF-AMS, *ACS Earth and Space Chemistry*, 3, 1451-1459, 2019.
1001 Zhang, M., Wang, X., Chen, J., Cheng, T., Wang, T., Yang, X., Gong, Y., Geng, F., and Chen,
1002 C.: Physical characterization of aerosol particles during the Chinese New Year's firework events,
1003 *Atmospheric Environment*, 44, 5191-5198, 2010.

1004

1005 **Table 1:** Summary of total and speciated concentrations before, during, and after the firework
 1006 event. Species are divided based on units (Total to Zn: $\mu\text{g m}^{-3}$; succinate to Se: ng m^{-3}).

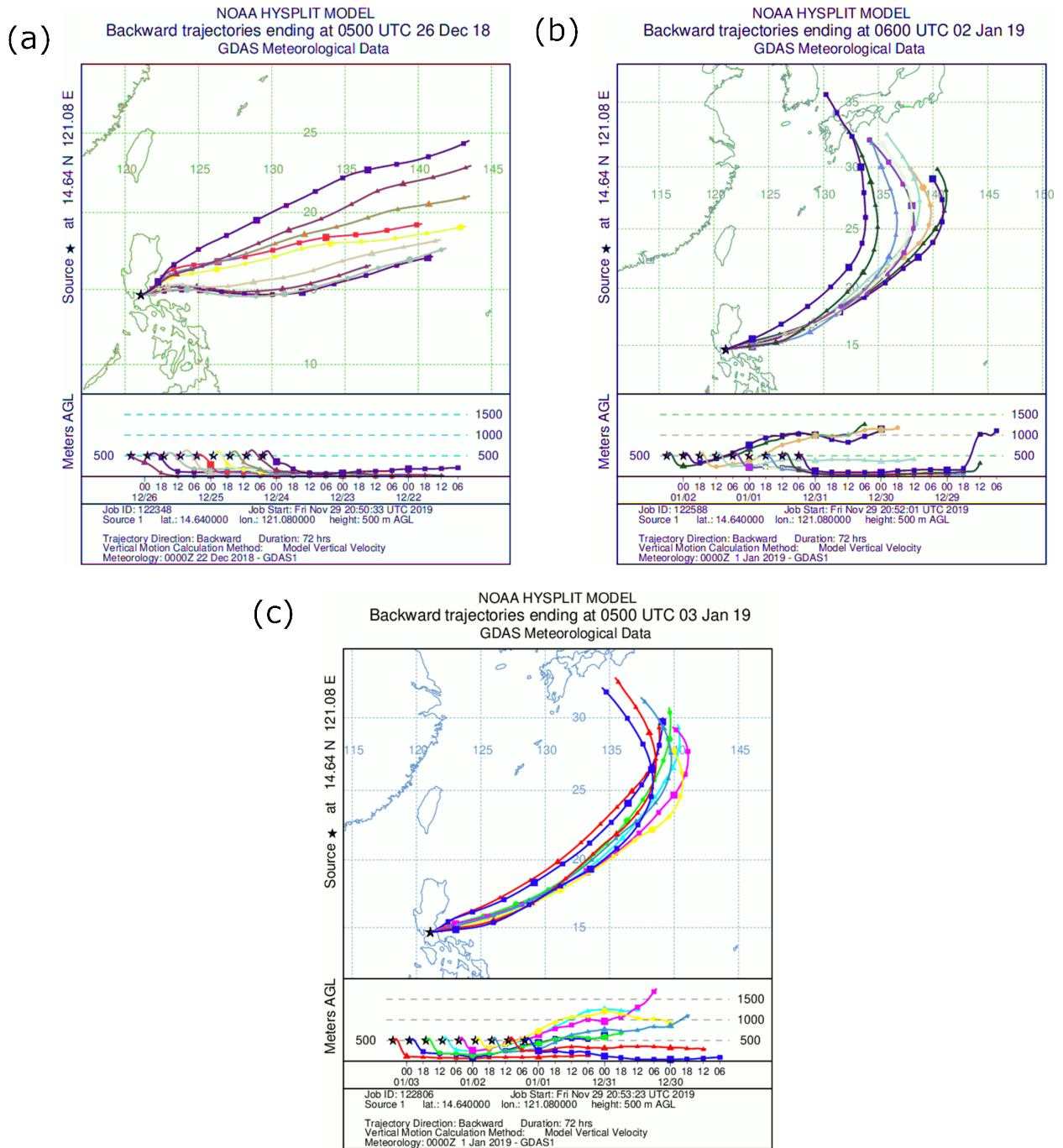
Species	Total Concentration			Species	Total Concentration		
	Before	During	After		Before	During	After
TOTAL	2.93	16.74	3.54	MSA	4.44	3.22	2.43
nss-SO₄²⁻	0.73	6.81	0.66	Mn	0.88	2.97	1.03
K⁺	0.37	5.05	0.25	Rb	0.62	1.24	0.25
NO₃⁻	0.64	1.70	0.65	Cr	0.16	1.01	0.29
Cl⁻	0.23	1.46	0.57	As	0.60	0.71	0.38
Mg²⁺	0.06	0.37	0.10	Ni	0.41	0.46	0.99
Na⁺	0.33	0.33	0.53	Ti	0.10	0.27	0.24
Ca²⁺	0.21	0.30	0.38	V	0.32	0.14	0.30
NH₄⁺	0.21	0.19	0.28	Mo	0.05	0.10	0.06
Ba	0.01	0.17	0.01	Cd	0.11	0.10	0.13
oxalate	0.10	0.12	0.06	Co	0.05	0.05	0.05
Cu	2.48E-04	6.89E-02	1.86E-03	Cs	0.02	0.02	0.01
Al	4.53E-03	0.05	0.01	Ag	0.02	0.02	4.00E-04
Sr	1.27E-03	4.65E-02	2.54E-03	Tl	0.01	0.02	1.80E-03
Zn	0.01	0.02	0.01	Zr	0.01	0.01	0.03
succinate	0.98	9.51	0	Sn	0.01	6.69E-04	0.03
Pb	1.68	8.33	1.03	Y	2.16E-04	4.56E-04	2.44E-03
phthalate	12.82	5.36	5.59	Nb	2.28E-04	1.59E-04	3.00E-04
adipate	5.35	4.83	11.73	Hf	0	0	2.18E-04
maleate	1.54	4.12	0	Hg	1.03E-03	0	0
Fe	2.91	3.47	7.32	Se	5.76	0	0

1007



1008

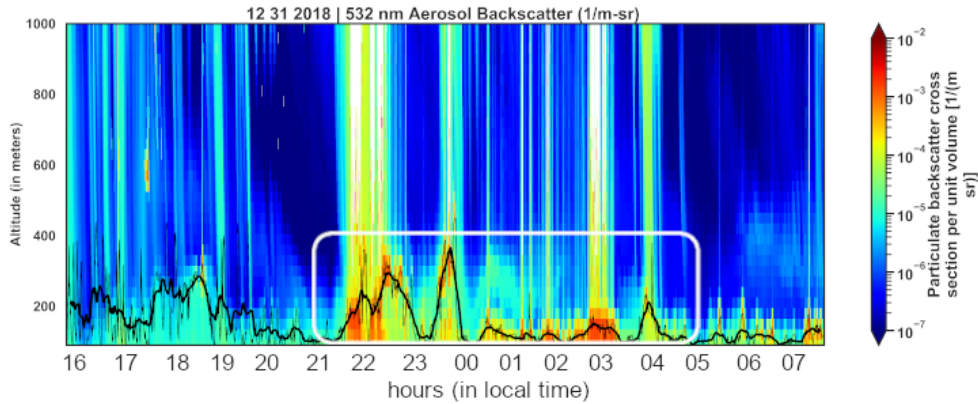
1009 **Figure 1:** (a) PM_{2.5} mass concentrations and rain accumulation at hourly resolution (local time,
 1010 dashed vertical line indicates midnight) as measured from the Manila Observatory main building
 1011 third floor rooftop (~88 m.a.s.l.) at the same period as the MOUDI size-specified samples during
 1012 the firework event. Ten-minute averaged values of (b) temperature and relative humidity, in
 1013 addition to (c) wind speed and direction. The wind barb legend in (c) shows how flags are added
 1014 to the staff with increasing wind speed and in the direction where the wind comes from. Figures
 1015 S2 and S3 show the hourly PM_{2.5} mass concentrations and ten-minute meteorological data before
 1016 and after the firework event, respectively.



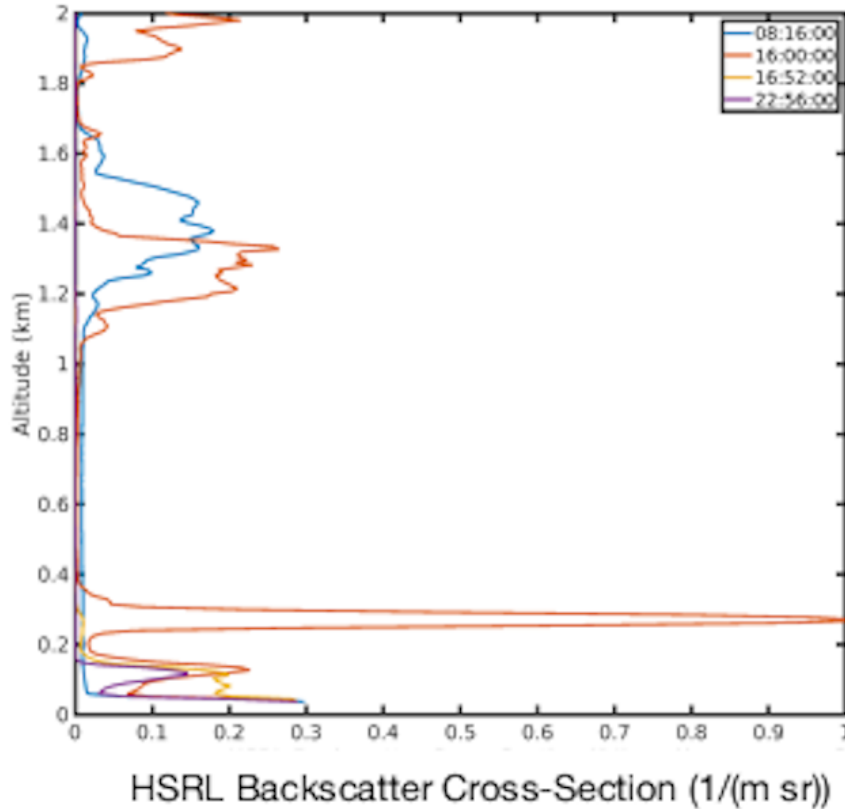
1017

1018 **Figure 2:** Three-day back trajectories with 6-h resolution for the periods (a) before, (b) during,
1019 and (c) after the firework event, ending at the point of the Manila Observatory at 500 m.

(a)



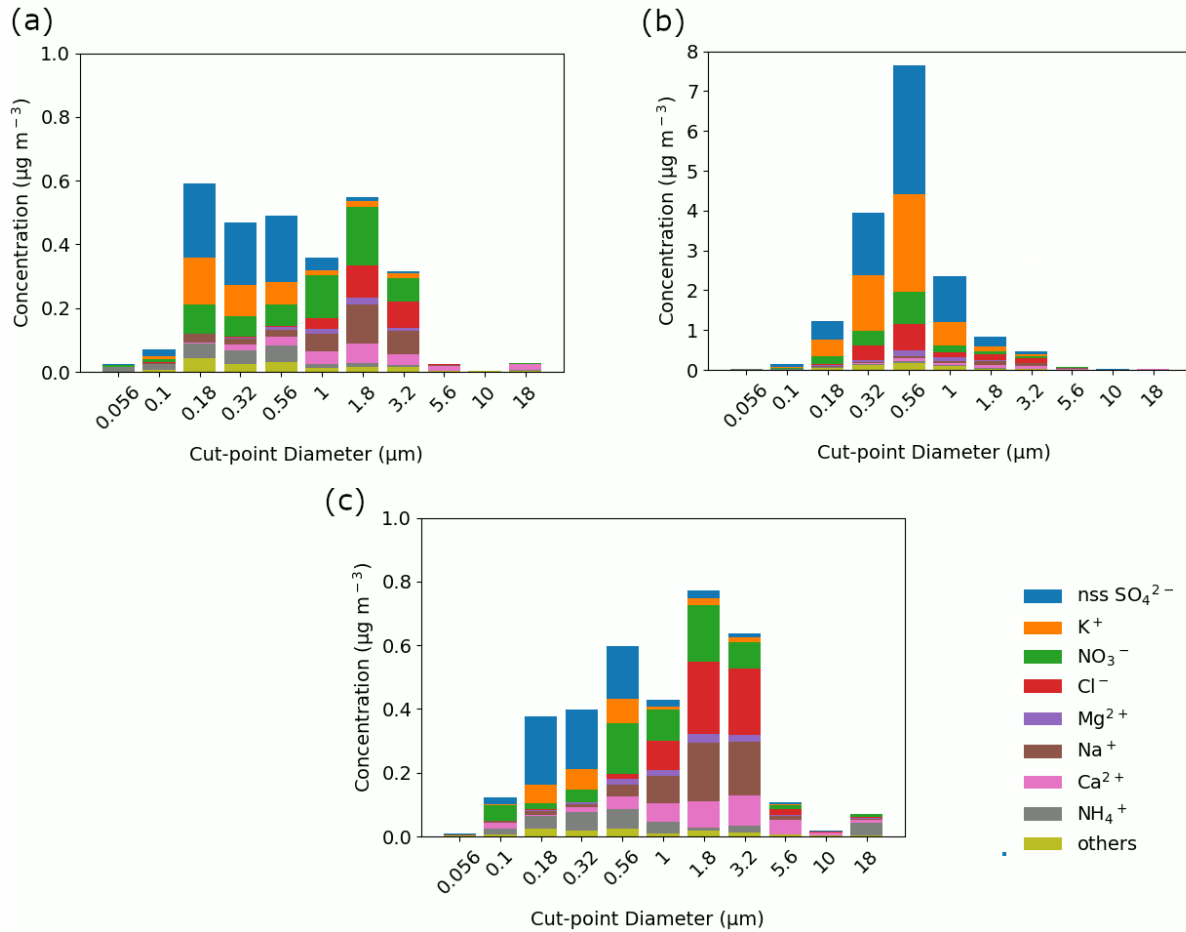
(b)



1020

1021 **Figure 3:** (a) Time series of the aerosol backscatter vertical profile from the High Spectral
1022 Resolution Layer (HSRL). The time shown is Universal Time (UT) and local time is UT + 8
1023 hours. The times circled by the white oval correspond to the peak of aerosol backscatter in the
1024 mixing layer due to firework activity. The approximate surface-attached aerosol layer height is
1025 shown as a thick black line. It is derived from a 30-min moving window average based on the 1-
1026 min values shown in thin black line (b) Vertical profiles of aerosol back-scatter at specific UT
1027 times of interest before, during, and after the fireworks.

1028



1030

1031

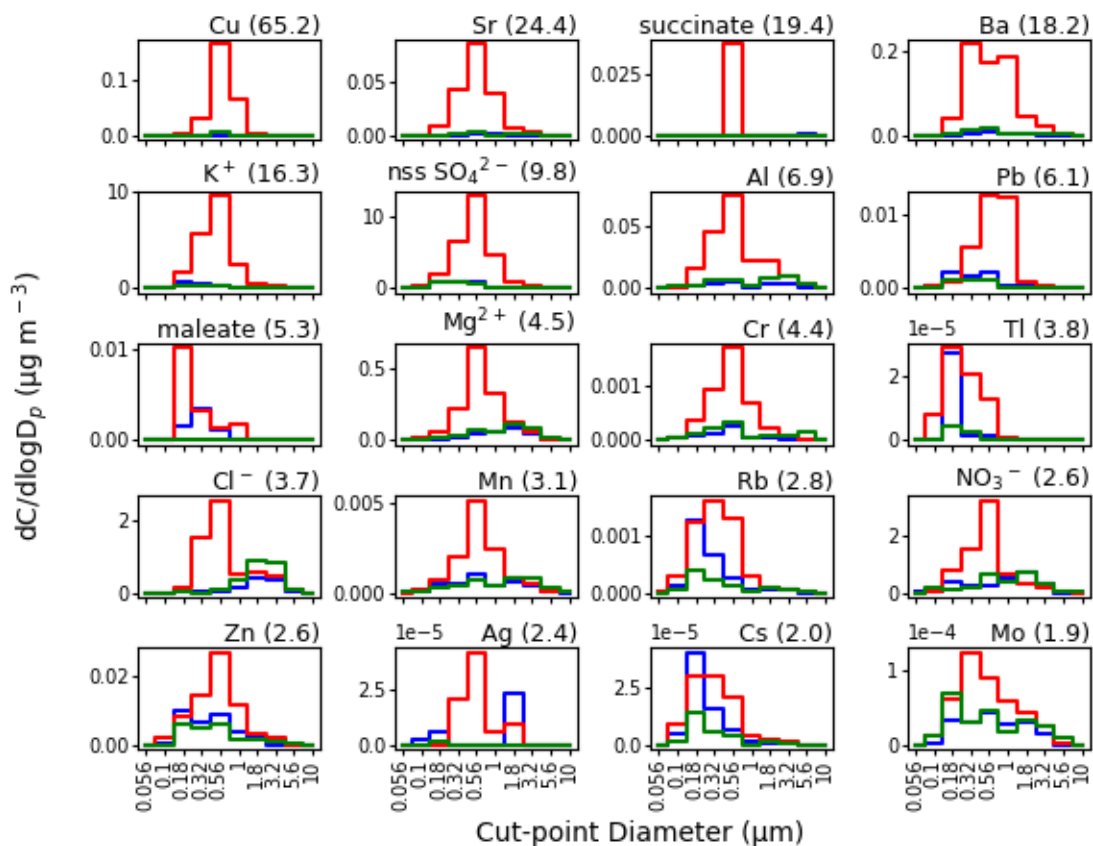
1032

1033

1034

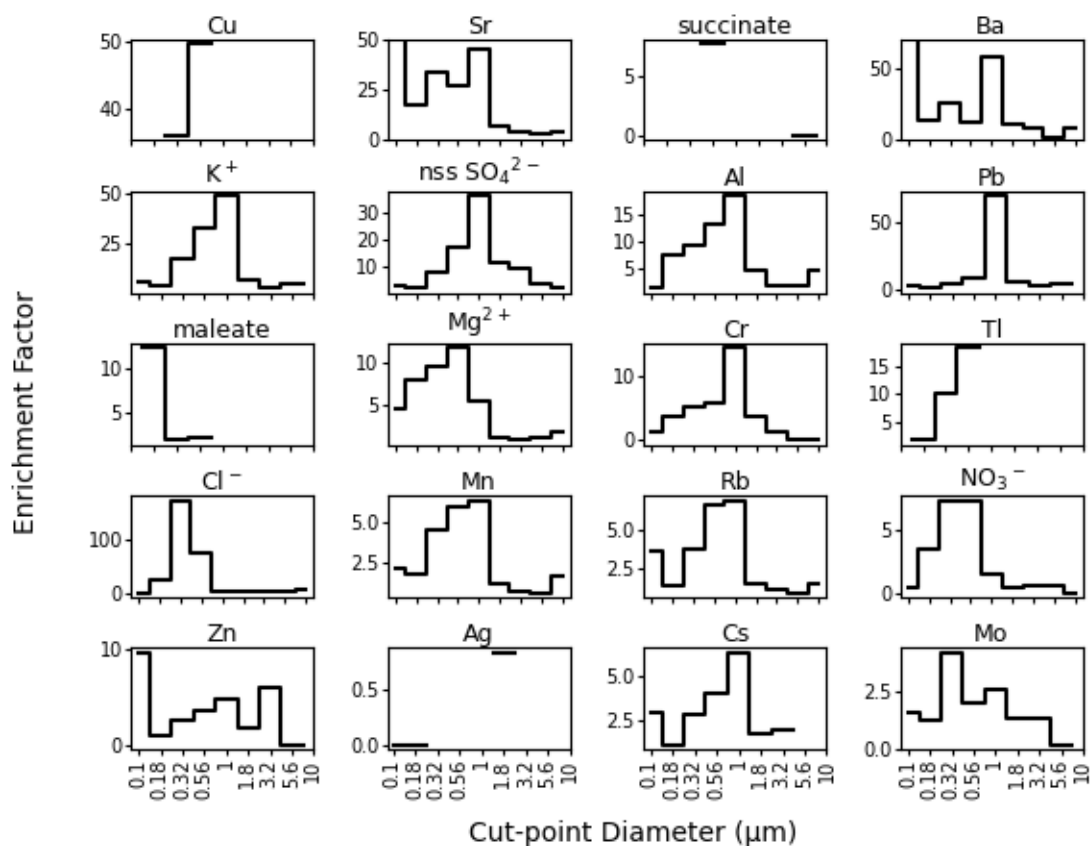
1035

Figure 4: Speciated mass size distributions of the major aerosol constituents measured (a) before, (b) during, and (c) after the firework event. Table 1 lists the bulk ($\geq 0.056 \mu\text{m}$) mass concentrations of these ions and elements, including those labeled here as “others” (Ba, oxalate, Cu, Al, Sr, Zn, succinate, Pb, phthalate, adipate, maleate, Fe, MSA, Mn, Rb, Cr, As, Ni, Ti, V, Mo, Cd, Co, Cs, Ag, Tl, Zr, Sn, Y, Nb, Hf, Hg, and Se).

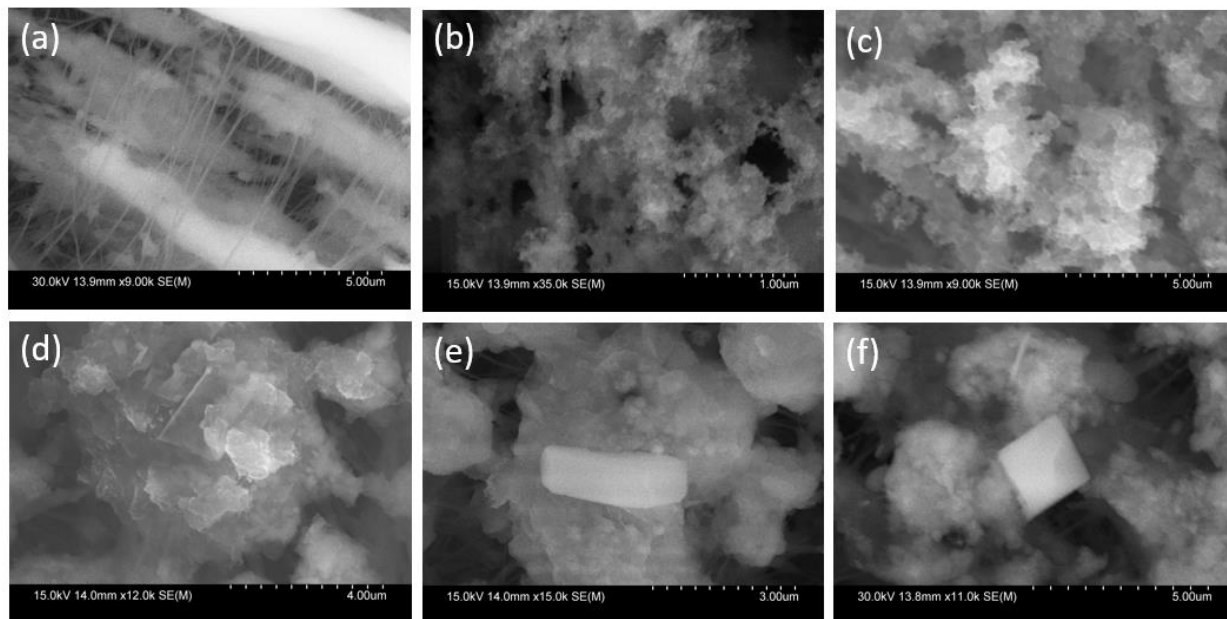


1036

1037 **Figure 5:** Speciated mass size distributions before (blue line), during (red line), and after (green
 1038 line) the firework event. Next to species labels are bulk ($\geq 0.056 \mu\text{m}$) mass concentration
 1039 enrichment values due to the firework event; species are shown with enrichments ≥ 1.9 . Figure S5
 1040 shows similar results for all other species.

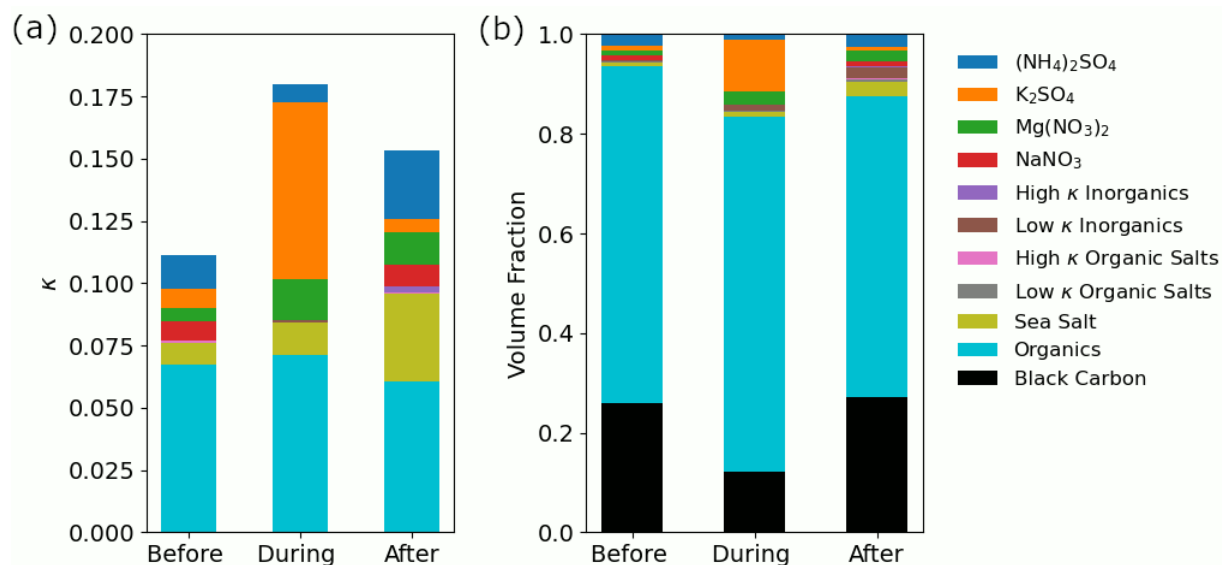


1041
 1042 **Figure 6:** Size-resolved enrichments for individual firework tracer species in order of decreasing
 1043 total bulk mass concentration enrichment (species from Fig. 5). Cut-point diameters with no
 1044 valid data are left blank. The y-axis of Sr and Ba are truncated to more easily show enrichments
 1045 in the larger size fractions. Figure S6 shows similar results for all other species.



1046

1047 **Figure 7:** Scanning electron microscope (SEM) images of (a) a blank PTFE (Teflon) substrate
1048 and (b-f) particles in different diameter ranges with firework influence: (b) 0.1 – 0.18 μm, (c)
1049 0.18 – 0.32 μm, (d) 0.32 – 0.56 μm, (e-f) 0.56 – 1.0 μm.



1050

1051 **Figure 8:** (a) Kappa (κ) values for the aerosol fraction between 0.056 – 3.2 μm before, during,
 1052 and after the firework event. The speciated contributions to the overall κ values (represented by
 1053 the colors) are categorized based on the classes of compounds in the legend following past work
 1054 (AzadiAghdam et al., 2019). Ammonium sulfate, K_2SO_4 , $\text{Mg}(\text{NO}_3)_2$, and NaNO_3 are high κ
 1055 inorganics but are plotted separately because of their large contributions. The speciated
 1056 contributions were calculated by multiplying the volume fraction of each compound class by its
 1057 intrinsic κ value (Table S4).